

# On idealized models of turbulent condensation in clouds

GUSTAVO C. ABADE

*Institute of Geophysics, Faculty of Physics, University of Warsaw, Poland*

**ABSTRACT:** Various microphysical models attempt to explain the occurrence of broad droplet size distributions (DSD) in clouds through approximate representations of the stochastic droplet growth by condensation in a turbulent environment. This work analyzes specific idealized models, where the variability of droplet growth conditions arises primarily from variability in the turbulent vertical velocity of the air carrying these droplets. Examples are the stochastic eddy hopping model operating in adiabatic parcels and certain types of DNS-like models. We show that such models produce droplet size statistics that are spatially inhomogeneous along the vertical direction, causing the predicted DSD to depend on the DSD spatial sampling scale  $\Delta$ . In these models,  $\Delta$  is implicitly related to the spatial extent of the droplets turbulent diffusion (approximated by Brownian-like excursions) and thus grows like  $t^{1/2}$ . This leads to spurious continuous DSD broadening, as the growth in time (also like  $t^{1/2}$ ) of the standard deviation of droplet squared radius arises essentially from the growth of the sampling scale  $\Delta$ . Also, the DSDs predicted by the models discussed here are not necessarily *locally* broad (in the sense that large and small droplets might not be well-mixed in sufficiently small volumes) and thus do not necessarily indicate enhanced probabilities of gravity-induced droplet coagulation. In the effort to build a firm physical basis for subgrid parametrizations, this study presents a framework to explain the merits and limitations of idealized models, indicating how to assess and use them wisely as a subgrid representation of turbulent condensation in large-eddy simulations of clouds.

**SIGNIFICANCE STATEMENT:** The droplet size distribution is a prime characteristic of a cloud, controlling the initiation of precipitation and how the cloud modulates solar radiation. Microphysical processes shaping the droplet size distribution, such as droplet growth by condensation in the turbulent cloud flow, occur on scales that are small compared with the resolution of the numerical models used to simulate the entire cloud. Such subgrid-scale aspects are incorporated in these models by parametrizations relating microphysical processes to the model variables. In the effort to build a firm physical basis for such parametrizations, this study analyzes idealized representations of turbulent condensation at subgrid-scales and presents a framework to explain the merits and limitations of these representations, indicating how to overcome their deficiencies.

## 1. Introduction

Adiabatic cloud parcel models and direct numerical simulations (DNS) of cloudy volumes with triply periodic boundary conditions (PBC) are widely used frameworks to study cloud microphysics. These idealized frameworks are designed to provide basic understanding of cloud processes occurring at small scales and eventually give insights into the central problem of subgrid-scale (SGS) modeling of cloud microphysics in large-eddy simulations (LES) of clouds.

The suitability of these idealized models to explain, in particular, the occurrence of local broad droplet size distributions in clouds has been recently questioned by Prabhakaran et al. (2022). Their objections concern models

where the variability of droplet growth conditions (determined by the supersaturation droplets experience) is due primarily to variability of the turbulent vertical velocity of the air carrying these droplets (through the adiabatic cooling effect). Examples of such models are the so-called eddy hopping model [e.g., Sardina et al. (2015); Grabowski and Abade (2017); Abade et al. (2018)] operating in adiabatic cloud parcels and a certain type of DNS-like models [e.g., Vaillancourt et al. (2002); Lanotte et al. (2009); Sardina et al. (2015, 2018); Saito and Gotoh (2018); Thomas et al. (2020); Grabowski et al. (2022b,a)].

The models mentioned above presumably predict broad droplet size distributions, in general qualitative agreement with *in situ* measurements. However, as we shall explain later, the predicted droplet size distributions are dependent on the sampling volume (which is generally unspecified) and cannot be generally regarded as *locally* broad. That is, large and small droplets, forming the left and right tails of the predicted distribution, might not be well-mixed in sufficiently small cloudy volumes. This feature is important because locally broad droplet size distributions accelerate the onset of the collision-coalescence process, as they enhance the probability of gravity-induced droplet collision due to differential sedimentation velocities of droplets having different sizes.

Idealized adiabatic cloud parcels and cloudy periodic boxes in DNS models, combined with some explicit treatment of the microphysics, are commonly regarded as instrumental models to represent the unresolved subgrid cloudy states in LES. This is based on the picture that the subgrid microphysical state of a particular grid box (of linear size  $\Delta$ ) consists of a statistical ensemble of the

---

Corresponding author: Gustavo Abade, [gustavo.abade@fuw.edu.pl](mailto:gustavo.abade@fuw.edu.pl)

microphysical states of adiabatic parcels or DNS periodic boxes (of characteristic size  $\Delta$ ) that instantaneously occupy the volume of this particular grid box. In this picture, there are two essential aspects associated with the characteristic size  $\Delta$ : (a) this is generally the scale on which the cloudy air in a grid box is assumed to acquire its mean turbulent kinetic energy  $k$  at the rate  $\varepsilon$  per unit mass; and (b) it specifies the linear extent of the *sampling volume* over which relevant microphysical characteristics, such as the droplet size distribution and its moments, are evaluated. One way to state the central issue we bring out in this paper is that the eddy hopping model and some DNS-like studies observe only the first aspect (a), that is,  $\Delta$  as the scale on which turbulent kinetic energy is supplied to the system, but inadvertently miss the second essential aspect (b), that  $\Delta$  also specifies the extent of the averaging volume. This omission results in “non-local” sampling of microphysical properties and arises from ill-suited boundary conditions, as well shall clarify later in this work. Issues with ill-suited boundary conditions used in these idealized models were indicated by Prabhakaran et al. (2022).

This work describes a framework to explain the deficiencies and merits of the idealized models of turbulent condensation mentioned above. The suggested framework addresses the specific comments of Prabhakaran et al. (2022) (see their Section 5.b) and assists us in properly sampling the droplet size statistics in idealized models, as we shall do for the eddy hopping model operating in adiabatic cloud parcels. In particular, understanding the deficiencies and merits of the eddy hopping model (as a stand-alone representation of turbulent condensation in adiabatic parcels) will motivate its wise use as a subgrid condensation model built in an LES scheme that employs particle-based microphysics. We also formulate a consistency condition for any subgrid model of turbulent condensation that (explicitly or not) includes turbulent vertical velocity fluctuations as one possible source of subgrid supersaturation variability.

Before we proceed with this program, some preliminary background is provided in Sec. 2, where we define the droplet size distribution (DSD) and discuss its dependence on the sampling volume. For clarity we outline in Sec. 3 the theoretical framework of Cooper (1989), which is based on the quasi-steady supersaturation approximation, and recall the *reversible condensation* scenario. This is a useful reference scenario where no strictly local DSD broadening is possible. The framework of Cooper (1989) incorporates many previous explanations [e.g., Bartlett and Jonas (1972); Manton (1979)] of the flaws in earlier versions of the stochastic condensation theory, which was revised and improved by Khvorostyanov and Curry (1999). In Section 4 we recall the essentials of the eddy hopping model operating in adiabatic parcels, explain its deficiencies and propose ways to enforce a correct *local sampling* of the DSD. Section 5 discusses deviations from the quasi-steady approximation and explores insights from the work

of Clark and Hall (1979) on possible ways in which DSD may become locally broad. Section 6 briefly reviews two types of DNS-like studies of turbulent condensation and explain that one of these types has the same deficiencies of the eddy hopping model. In Section 7 we discuss some aspects that emerge when idealized stochastic models (in particular, the eddy hopping model) are used as a subgrid condensation scheme in LES of clouds with particle-based microphysics. In Sec. 8 we summarize the main points of this work.

## 2. Fine-grained and filtered DSD

The fundamental characteristic of a cloudy volume considered in this work is the droplet size distribution (DSD). Because it may depend on the volume over which the distribution is averaged, every well-defined DSD goes with the specification of its underlying spatial averaging scale.

Here we define the *local* or fine-grained DSD  $n(r; \mathbf{x}, t)$  in such a way that

$$n(r; \mathbf{x}, t) d\mathbf{x}, \quad (1)$$

is the number of droplets that lie in the volume element  $d\mathbf{x}$  around  $\mathbf{x}$  at time  $t$  and that have a radius in the range  $[r, r + dr]$ . This definition implicitly incorporates the *continuum hypothesis* for the disperse liquid phase in the cloudy air. Thus *local* refers to the mathematically infinitesimal volume element  $d\mathbf{x}$  of a particular “physical point” in the continuous cloud. This physical point is assumed to be “macroscopically infinitesimal”, but at the same time “mesoscopically infinite” [following analogous considerations by Résibois and De Leener (1977) while defining regular distribution functions used in the kinetic theory of gases]. This means that such a physical point is small enough for all microphysical properties of the cloudy air not vary appreciably over the extension of the sampling volume  $d\mathbf{x}$ , but at the same time big enough to contain a large number of droplets.

The fine-grained DSD discussed above is thus the local size distribution in a continuous description of cloudy air. However, the continuous equations of cloudy air motion are intractable except by numerical methods. These methods require spatial discretization that naturally introduces a cutoff lengthscale  $\Delta$  determining the finite spatial resolution of the numerical model. In an LES setting,  $\Delta$  may be loosely identified with the size of the computational grid box. A grid box is considered a “point” in the spatially discretized LES domain. Thus the “local” DSD at this “grid point” is actually a spatially filtered DSD,

$$\langle n(r; \mathbf{x}, t) \rangle_{\Delta} = \int G(\mathbf{x} - \mathbf{x}') n(r; \mathbf{x}', t) d\mathbf{x}', \quad (2)$$

where  $G$  is a spatial filter function of characteristic filter width  $\Delta$  and satisfies  $\int G(\mathbf{x}) d\mathbf{x} = 1$  [see e.g., Germano

(1992)]. (In the limit of  $\Delta \rightarrow 0$ , the filter function  $G$  tends to the Dirac delta distribution.) We note that LES generally does not define the filter function  $G$  explicitly; an implicit filter arises from the spatial discretization. Thus the distribution  $\langle n(r) \rangle_\Delta$  is simply the grid average (or the  $G$ -weighted spatial average) of the fine-grained  $n(r)$ , where  $\Delta$  is the spatial averaging lengthscale. Also, we define  $\mu_k = \int r^k n(r) dr$  as the  $k$ th moment of the fine-grained DSD  $n(r)$  and  $\langle \mu_k \rangle_\Delta = \int r^k \langle n(r) \rangle_\Delta dr$  is the corresponding moment of the filtered DSD  $\langle n(r) \rangle_\Delta$  with filter width  $\Delta$ . The fine-grained variance of  $r$ , we denote by  $\sigma_r(0)$ , is proportional to  $\mu_2 - \mu_1^2$  (up to a normalization constant), and  $\sigma_r(\Delta) \propto \langle \mu_2 \rangle_\Delta - \langle \mu_1 \rangle_\Delta^2$  is the filtered variance of  $r$ .

We note that the moments  $\mu_k$  and  $\langle \mu_k \rangle_\Delta$  are *ensemble averages*, which are averages over realizations, the observation point being fixed. The spatial filtering specifies the sampling volume around the observation point. That is, the ensemble average we consider is *conditional*. The ensemble average at a given observation point  $\mathbf{x}$  is computed over the droplet sizes *conditional* on droplets positions being inside a given sampling *volume* around  $\mathbf{x}$ . This sampling volume can be: (a)  $d\mathbf{x}$  around  $\mathbf{x}$  (the “physical point” under the approximation of a continuous cloud) or (b) a finite volume  $\Delta^3$  (the volume of the grid box) around a grid point  $\mathbf{x}$  in a simulation setting with spatial resolution  $\Delta$ . The conditional sampling in (a) corresponds to the fine-grained DSD, and the conditional sampling (b) corresponds to the filtered DSD with filter width  $\Delta$  we discussed above.

Also, if  $\Delta$  is large (compared to a lengthscale we shall define later in Sec. 3), the “grid point” may no longer be considered mathematically infinitesimal as the “physical point”, and the filtered DSD  $\langle n(r) \rangle_\Delta$  may incorporate variation due to spatial distribution of the fine-grained DSD. Thus fine-grained DSDs that are locally narrow in a theoretical physical point may produce filtered DSDs that are locally broad in a computational grid point.

### 3. The reversible condensation regime

A useful theoretical framework to study the DSD formation was developed by Cooper (1989). His analysis incorporates the findings of earlier works [e.g., Bartlett and Jonas (1972) and Manton (1979)] that rule out (under certain conditions) turbulence-induced vertical velocity fluctuations as the cause of strictly local DSD broadening. For clarity, we reproduce below some essential points of Cooper (1989) and make some remarks. A general one is that theories attempting to explain DSD broadening usually do not explicitly specify the sampling volume or spatial averaging length scale  $\Delta$  underlying the examined DSD. We attempt to make this clear while recalling the *statistical ensemble* specified by Cooper (1989).

We follow Cooper (1989) closely and assume that each droplet of radius squared  $a = r^2$  grows according to

$$\frac{da}{dt} = 2DS(t), \quad (3)$$

where  $S$  is the supersaturation experienced by the droplet and  $D$  is the effective diffusion coefficient (here assumed constant for simplicity). Surface tension and solute effects were neglected.

Cooper (1989) then proceeds by assuming the supersaturation  $S(t)$  has approached its quasi-steady value  $S_{qs}$ ,

$$S \approx S_{qs} \equiv A_1 \tau_{ph} w, \quad (4)$$

where  $w$  is vertical velocity of the air parcel surrounding the droplet ( $A_1$  depends weakly on temperature and may be considered constant to a good approximation),  $\tau_{ph} = 1/(A_2 \mu_1)$  is the phase relaxation time,  $\mu_1$  is the first moment of the DSD, and  $A_2$  is a constant.  $\tau_{ph}$  is the time constant for the exponential approach of  $S(t)$  to  $S_{qs}$  and characterizes the local structure of the cloudy environment where the droplet grows. Although (4) is not valid everywhere (e.g., near the cloud base), the quasi-steady regime is a useful limit for analysis.

The first moment  $\mu_1$  specifying  $\tau_{ph}$  can be written as  $\mu_1 = N \langle r \rangle$ , where  $N = \mu_0$  is the droplet number concentration (corresponding to the zeroth moment  $\mu_0$  of the DSD), and  $\langle r \rangle = \mu_1/N$  is the mean droplet radius. The sampling volume underlying  $\mu_1$  and  $\mu_0$  (and hence  $N$  and  $\langle r \rangle$ ) was not explicitly specified in Cooper (1989), thus we assume here that  $\mu_1$  and  $\mu_0$  are moments of the fine-grained DSD defined in Sec. 2.

The idealized models of turbulent condensation we will discuss here assume that

$$\tau_{ph} \approx \bar{\tau}_{ph} \equiv 1/[A_2 \langle \mu_1 \rangle_\Delta], \quad (5)$$

where  $\Delta$  is the characteristic size of the sampling volume that include all droplets of the ensemble.

We also assume that the droplets are suspended and follow the air flow as tracers (droplet-tracer limit). Then the vertical component  $z$  of the droplet position is related to the velocity  $w$  by

$$dz = w(t) dt. \quad (6)$$

and hence

$$da \approx \bar{\gamma}_a dz, \quad \bar{\gamma}_a \equiv 2DA_1 \bar{\tau}_{ph}. \quad (7)$$

Now consider a droplet that at time  $t_0$  has been activated with activation squared radius  $a_0$  at the cloud base located at  $z_0$ . Under the assumptions above, the droplet squared radius at time  $t > t_0$  for a droplet located at  $Z(t) > z_0$  is

$$a[Z(t)] \approx a_{rev}[Z(t)],$$

where

$$a_{\text{rev}}(z) \equiv a_0 + \bar{\gamma}_a(z - z_0), \quad (8)$$

is the *reversible* squared radius. For fixed  $a_0$  and  $z_0$ , Eq. (8) is a *one-to-one relation* between the droplet squared radius  $a$  and the droplet vertical position  $z$ . This defines the scenario of perfectly *reversible condensation*<sup>1</sup>.

To discuss any characteristics of a droplet size distribution, we need to specify its underlying *statistical ensemble*. The ensemble used by Cooper (1989) is comprised by all droplets reaching a given height  $z$  at a particular time  $t$  after being activated at time  $t_0$  (with squared-radius  $a_0$ ) while crossing the cloud base located at  $z_0$ . Also all droplet in the ensemble experiences the same constant phase relaxation time  $\bar{\tau}_{\text{ph}}$ . Thus for this ensemble, Eq. (8) implies no variability in  $a_{\text{rev}}$  at a particular height  $z$  and the variance of  $a_{\text{rev}}$  vanishes there,

$$\sigma_a^2(z, t) = \langle [a_{\text{rev}} - \langle a_{\text{rev}} \rangle]^2 \rangle = 0. \quad (9)$$

We emphasize that the angle brackets  $\langle \cdot \rangle$  in (9) denote an average over the ensemble of cloud droplets all having  $Z(t) = z$  at time  $t$  and having the same activation area  $a_0$  at the same activation level  $z_0$ .

The scenario of *reversible condensation* above is thus defined by three main assumptions: (a) quasi-steady supersaturation, (b) lack of variability in the phase relaxation time  $\tau_{\text{ph}}$  among the droplets in the ensemble, and (c) the droplets are suspended and follow the air flow as tracers (i.e., droplet inertia and sedimentation are neglected). This third assumption is not made explicit in the analysis of Cooper (1989).

This reversible condensation scenario will serve as a reference limit, where the droplet squared radius  $a$  is *maximally correlated* with its vertical position  $z$  inside the cloud. Deviations from any of the assumptions (a) to (c) listed above will work to destroy the one-to-one relation between  $a$  and  $z$ , thus creating conditions for broadening of the local (fine-grained) DSD.

#### a. “Point” and extended ensembles

In the Cooper’s ensemble discussed above, the ensemble averaging in Eq. (9) implicitly assumes  $\Delta \rightarrow 0$  as the ensemble considers droplets reaching a particular *point* (at height  $z$ ) and forming the DSD there. Thus  $\sigma_a^2(z, t)$  in Eq. (9) is the fine-grained variance  $\sigma_a^2(0)$  at a “physical point” in the continuous cloud in the sense discussed in Sec. 2.

<sup>1</sup>Consider a droplet of initial squared radius  $a(t_0)$  ascending with a time-dependent vertical velocity  $w(t)$  for a certain time  $t_0 \leq t \leq t_1$ . Now reverse the vertical velocity by setting  $w(t) = -w[2(t_1 - t_0) - t]$  in  $t_1 \leq t \leq 2(t_1 - t_0)$ . Under the reversible condensation regime, not only the droplet vertical motion will reverse, but its growth history reverses as well because  $da \propto w(t)dt$ . Hence its squared radius returns to its starting value  $a(t_0)$ .

Figure 1.a shows the ensemble of droplets that reach a given height  $z$  at a particular time  $t$ . There, fluctuations in the updraft velocity only cannot support broadening of the fine-grained DSD in the regime of reversible condensation.

The situation is different in a simulation setting, where the sampling volume is finite and defined by the length scale of the smallest spatial variation resolved by the model. This motivates us to extend Cooper’s “point” ensemble by considering the droplets that at time  $t$  reach a height in the range  $[z - \Delta/2, z + \Delta/2]$ , where  $\Delta$  is of order of a typical vertical length scale resolution used in LES. This ensemble is illustrated in Fig. 1.b. For this extended ensemble, the broad filtered DSD (with filter width  $\Delta$ ) obtained in the reversible condensation scenario arises from the increase in droplet squared radius with height over the averaging length scale  $\Delta$  [Eq. (8)].

In principle, any particle-based SGS model for condensation built in LES should capture this variability in the droplet squared radius (at least under a regime of nearly reversible condensation). However, this variability is smeared out when the SGS microphysical scheme assumes all droplets in a given grid box experience the same grid-mean supersaturation  $\langle S \rangle$ , as this subgrid *uniform condensation* tends to narrow the filtered DSD.

It is evident that the breadth of the local filtered DSD will depend on  $\Delta$  when  $\Delta$  is of the same order or larger than the length scale

$$H_a \equiv \sigma_a(0) / |\partial a_{\text{rev}}| = \sigma_a(0) / \bar{\gamma}_a, \quad (10)$$

where  $\sigma_a(0)$  denotes the *fine-grained* standard deviation of the droplet squared radius (corresponding to a vanishing sampling volume or filter width  $\Delta \rightarrow 0$ ). Then  $H_a$  is the length scale over which the reversible squared radius  $a_{\text{rev}}$  changes by a value  $\sim \sigma_a(0)$  along the vertical direction. Thus for  $\Delta \gtrsim H_a$ , the filtered DSD with filter width  $\Delta$  will incorporate variation due to spatial distribution of the fine-grained DSD and  $\sigma_a(\Delta)$  will appreciably differ from  $\sigma_a(0)$ .

Later in this work we use Cooper’s framework and the reference reversible condensation scenario outlined above to discuss the current limitations of two idealized frameworks, namely the so-called eddy hopping model operating in adiabatic parcels and certain DNS-like models, where microphysical variability is driven by local velocity fluctuations.

## 4. Models operating in adiabatic cloud parcels

The standard theory of droplet growth by condensation in an adiabatic cloud parcel assumes uniform condensation, where all droplets in the parcel experience the same supersaturation. This approximation produces narrow DSDs in disagreement with *in situ* measurements of broad droplet spectra in clouds [see e.g., Shaw (2003)].

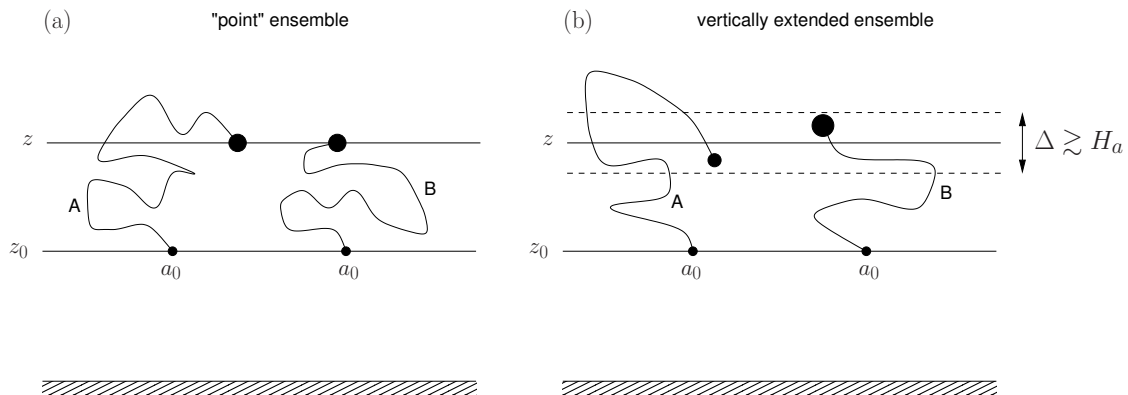


FIG. 1. Schematic representation of (a) the “point” ensemble ( $\Delta \rightarrow 0$ ), and (b) the vertically extended ensemble (finite  $\Delta$ ) in an idealized cloud with reversible condensation. Two droplets undergoing distinct trajectories (labeled A and B) but arriving at the same particular height  $z$  will have the same radius [panel (a)]. The breadth of the resulting fine-grained DSD vanishes. If the sampling volume is extended vertically to have a thickness  $\Delta$ , then at a given time  $t$  this sampling volume may accommodate droplets arriving at different heights in the range  $[z - \Delta/2, z + \Delta/2]$  and thus having different radii [panel (b)]. The broad filtered DSD (with filter width  $\Delta$ ) obtained under the reversible condensation regime [panel (b)] arises from the increase of droplet size with height [Eq. (8)] over the averaging length scale  $\Delta$ .

Attempts to resolve this paradox attributes the occurrence of broad droplet size spectra in clouds to the stochastic droplet growth by condensation in a turbulent environment [see e.g., Khvorostyanov and Curry (1999)]. An approximate account of turbulent effects on condensation in the adiabatic cloud parcel framework was done by Sardina et al. (2015), Grabowski and Abade (2017) and Abade et al. (2018). These so-called eddy hopping models use a Lagrangian (particle-based) stochastic treatment of the droplet growth and presumably predict a broad DSD.

A much earlier numerical study by Bartlett and Jonas (1972) attempted to account for the effects of turbulence by subjecting the adiabatic cloud parcel to a time-dependent updraft. Their study ruled out turbulence-induced vertical velocity fluctuations as the cause of strictly local DSD broadening. Then why does the eddy hopping model (Sardina et al. 2015; Grabowski and Abade 2017; Abade et al. 2018) predict broad DSDs, while Bartlett and Jonas (1972) do not?

The essential difference between these two approaches lies in the statistical ensemble over which the DSD is sampled. The ensemble in Bartlett and Jonas (1972) corresponds to the “point” ensemble (Fig. 1a) with infinitesimal sampling length scale ( $\Delta \rightarrow 0$ ), and thus provides the *fine-grained* DSD. In contrast, the eddy hopping model considers the extended ensemble (Fig. 1b) with finite sampling length scale, and thus provides the *filtered* DSD with filter width  $\Delta \gtrsim H_a$ . While the fine-grained DSD of Bartlett and Jonas (1972) is narrow, the filtered DSD predicted by the eddy hopping model is broad.

Next we discuss the eddy hopping model in more detail and explain a major artifact in Sardina et al. (2015); Grabowski and Abade (2017); Abade et al. (2018). This artifact makes the variance of the filtered DSD in the adi-

abatic parcel to continuously grow in time. We show that this growth does not reflect an actual local DSD broadening with time but results from the growth in time of the filter width  $\Delta$  underlying the examined DSD.

#### a. Eddy hopping model and nonlocal DSD sampling

The eddy hopping model considers an ensemble of representative cloud droplets. The model describes the evolution of four variables attached to each droplet: its squared radius  $a$ , the supersaturation  $S$  the droplet experiences, its vertical position  $z$  and its vertical velocity  $w$ . The evolution of the state variables  $(a, S, w, z)$  is described by the following set of equations:

$$\frac{da}{dt} = 2DS, \quad (11)$$

$$\frac{dS}{dt} = -\frac{S}{\tau_s} + A_1 w, \quad (12)$$

$$dw = -\frac{w}{\tau_w} dt + \sqrt{\frac{2\sigma_w^2}{\tau_w}} dW(t), \quad (13)$$

$$dz = w dt. \quad (14)$$

The equations above include a set of model parameters  $(\tau_s, \tau_w, \sigma_w)$  we shall specify later.

The identifying feature of the eddy hopping model is that the supersaturation evolving according to (12) is forced by vertical velocity  $w$  via the adiabatic cooling of the ascending air surrounding the cloud droplet. The vertical velocity  $w$  is described by Eq. (13), where  $\tau_w$  is the Lagrangian integral timescale of  $w$ , and  $dW(t)$  is the increment of a Wiener process [see e.g., Rodean (1996)]. The latter introduces the “noise” due to turbulent fluctuations.

Equation (13) serves as a coarse representation of the vertical velocity fluctuations of a fluid particle due to a range of homogeneous isotropic turbulence eddies of sizes smaller than a characteristic length  $\Delta$ . This is the length scale on which the cloud parcel, filled with homogeneous turbulence, is imagined to acquire its mean turbulent kinetic energy  $k$  ( $= 3\sigma_w^2/2$ ) at a given rate  $\varepsilon$  per unit mass.

Assuming that turbulent cloud parcels may provide insights into subgrid modeling of the microphysics in large-eddy simulations (LES) of clouds, it is reasonable to assume that  $\Delta$  has the size of a typical LES grid box. Thus  $\Delta$  lies in the inertial range of cloud turbulence and usually varies from several meters to several tens of meters.

Equation (12) for the supersaturation may be cast into the form

$$\frac{dS}{dt} = -\frac{S - S_{qs}}{\tau_s}, \quad (15)$$

to make it explicit that  $S$  relaxes to the quasi-steady value  $S_{qs} = A_1 \tau_s w$  with time constant  $\tau_s$  — the supersaturation relaxation time. The time constant  $\tau_s$  is a model parameter defined as the harmonic mean of the phase relaxation time  $\tau_{ph}$  and the relaxation time  $\tau_{mix}$  associated with turbulent mixing,  $\tau_s = 1/(\tau_{ph}^{-1} + \tau_{mix}^{-1})$ . We commonly assume  $\tau_{mix} \approx \tau_w$ .

For times sufficiently longer than  $\tau_s$ , the supersaturation has attained its quasi-steady value  $S \approx S_{qs}$  which is proportional to  $w(t)$  [as in Eq. (4)]. Then it follows from (14) that the increment  $da$  in the droplet squared radius is closely related to the increment  $dz$  in its vertical position,

$$da \approx \bar{\gamma}_a dz, \quad (16)$$

where  $\bar{\gamma}_a = 2DA_1\tau_s$  and we have assumed that  $\tau_s$  is the same for all representative droplets in the ensemble.

Also, it follows from Eqs. (13) and (14) that (for times sufficiently longer than  $\tau_w$ ) the mean squared displacement along the vertical direction grows like [see e.g., Lemons (2002)]

$$\langle [z(t) - \langle z \rangle]^2 \rangle \sim t, \quad (17)$$

being the average  $\langle \dots \rangle$  calculated over all the representative cloud droplets. Thus the relation (16) implies that the variance  $\sigma_a^2$  of droplet squared radius grows according to the same scaling,

$$\sigma_a^2 = \langle [a(t) - \langle a \rangle]^2 \rangle \sim t, \quad (18)$$

when the average is computed over the same ensemble of representative droplets.

In conclusion, the eddy hopping model predicts continuous DSD broadening as the variance  $\sigma_a^2$  grows with time (Sardina et al. 2015). However, this broadening is *non-local* in a sense to be explained soon below. This non-local feature underlying the continuous growth of  $\sigma_a$  was overlooked by Sardina et al. (2015); Grabowski and

Abade (2017); Abade et al. (2018) because they inadvertently omitted Eq. (14) from their description.

The fluctuating vertical velocity  $w$  that drives supersaturation fluctuations  $S$  also drives the vertical dispersion of cloud particles. The spatial extent of this droplet dispersion is measured by the mean squared displacement (17). Thus the associated length scale

$$\tilde{\Delta}(t) = \langle [z(t) - \langle z \rangle]^2 \rangle^{1/2} \sim t^{1/2}, \quad (19)$$

which may be understood as the linear size of the sampling volume containing the whole droplet population in the parcel, grows with the square root of time. The sampling length scale  $\tilde{\Delta}(t)$  is not bounded and may eventually exceed the fixed scale  $\Delta$  on which energy is assumed to be supplied to the turbulence filling the parcel. We refer to this as a *non-local sampling* of the DSD in the eddy hopping model as illustrated schematically in Fig. 2.a. Figure 3 shows numerical results for the continuous droplet dispersion along the vertical extrapolating  $\Delta$  [gray dots in panels (a) and (b)] and the corresponding continuous growth of the standard deviation  $\sigma_a[\tilde{\Delta}(t)]$  [gray line in panel (c)].

#### b. Enforcing local sampling of the DSD

For the eddy hopping model to be relevant as an SGS stochastic condensation scheme in LES, then  $\tilde{\Delta}$  (the linear extent of the volume over which droplet size statistics is sampled) should be bounded to  $\Delta$ . This ensures a well-defined filtered variance  $\sigma_a^2(\Delta)$  that refers to the droplet population inside a grid box of size  $\Delta$ . This motivates us to enforce local sampling of the DSD in the adiabatic parcel and DNS-like frameworks as well.

We consider three different ways of imposing local DSD sampling depending on the framework where the eddy hopping model operates.

First, we may sample the droplet size statistics over a *subensemble* of cloud particles all having vertical position  $Z(t)$  between  $\langle z \rangle - \Delta/2$  and  $\langle z \rangle + \Delta/2$ , as illustrated in Fig. 2.b. This approach can be used in LES (as we shall discuss in Sec. 7), but is it impractical in the adiabatic parcel and DNS-like frameworks, because the number of droplets in the subensemble decays with time as droplets disperse and leave the sampling volume.

A second approach for local sampling is by using reflecting boundary conditions on  $z$  and  $w$  at the bottom and top horizontal boundaries of the sampling volume. These boundaries are separated by a constant distance equal to  $\Delta$ , thus enforcing  $\tilde{\Delta} = \Delta$  as illustrated in Fig. 2.b. This treatment was used by Abade and Albuquerque (2024) in an extended version of the eddy hopping model operating in mixed-phase adiabatic parcels. Reflecting boundary conditions preserve the number of representative droplets in the sampling volume. However it can be used only in the adiabatic parcel framework under the reversible condensation regime.

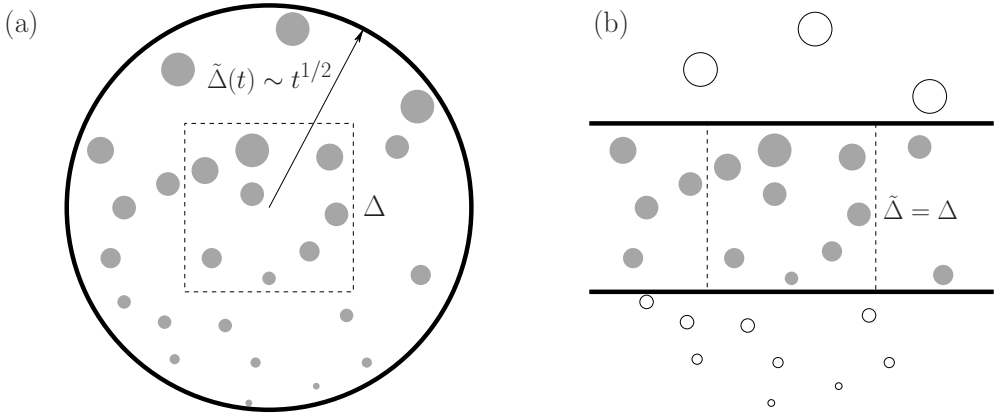


FIG. 2. (a) Non-local sampling in a turbulent adiabatic parcel, where the linear extent  $\tilde{\Delta}(t)$  of the implicit sampling volume grows like  $\sim t^{1/2}$  due to turbulent diffusion of cloud particles in all directions. As time increases,  $\tilde{\Delta}(t)$  becomes larger than the characteristic length scale  $\Delta$  on which the parcel acquires its turbulent kinetic energy. The same problem occurs in DNS-like models with usual periodic boundary conditions (PBC) in the vertical direction (see discussion in Sec. 6). (b) Adiabatic parcel with DSD statistics sampled over a subensemble of droplets (in gray) using proper boundary conditions at the top and bottom to enforce local sampling (see text for details).

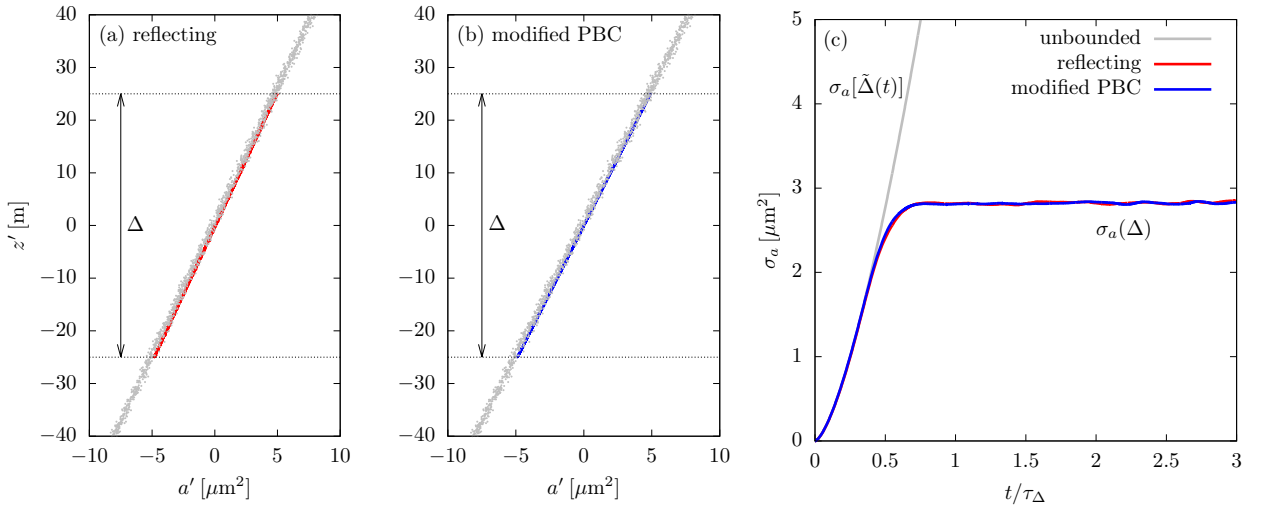


FIG. 3. [Panels (a) and (b)] Scatterplots of  $a' = a - \langle a \rangle$  and  $z' = z - \langle z \rangle$  to illustrate the local sampling in an adiabatic parcel of size  $\Delta$  enforced by using (a) reflecting boundary conditions (red dots) and (b) modified periodic boundary conditions (blue dots). Gray dots in panels (a) and (b) are for an unbounded sampling volume (non-local sampling) of growing length  $\tilde{\Delta}(t) \sim t^{1/2}$ . The results consider the reversible condensation regime. Panel (c) shows the time evolution ( $\tau_\Delta = \varepsilon^{-1/3} \Delta^{2/3}$ ) of the filtered standard deviation  $\sigma_a(\Delta)$  for fixed filter width  $\Delta$  (reflecting top and bottom walls and modified PBC), while  $\sigma_a[\tilde{\Delta}(t)]$  continuously grows along with the sampling length scale  $\tilde{\Delta}(t)$  in the unbounded case. Simulations are for  $N = 100 \text{ cm}^{-3}$ ,  $\varepsilon = 10^{-3} \text{ m}^2 \text{ s}^{-3}$ ,  $\langle S \rangle = 0$ , and  $\langle a \rangle = a_0 = 100 \mu\text{m}^2$ .

A third approach is the use of so-called *modified* periodic boundary conditions (PBC) in the vertical direction to be explained below. As Equation (16) and Figures 2, 3.a, 3.b indicate, the sampling volume containing droplets is embedded in a cloud which has a mean squared radius gradient  $\bar{\gamma}_a$  ( $\approx \partial_z a_{\text{rev}} = 2DA_1\tau_s$ ) in the  $z$ -direction. This resembles non-equilibrium (particle-based) molecular dynamics simulations of a fluid under shear (Lees and Edwards 1972) with constant velocity gradient  $\gamma_u = du/dz$  in the

$z$ -direction<sup>2</sup>. In this case, PBC must be used not only on particle positions, but on particle velocities as well (Lees and Edwards 1972).

In our turbulent condensation problem, modified PBC (in contrast to *usual* PBC) remaps not only droplets vertical positions, but also adjusts the droplets radii as droplets

<sup>2</sup>In molecular dynamics simulations of fluid under shear, the sampling volume containing the particles is considered as being embedded in a fluid which has a constant velocity gradient  $\gamma_u = du/dz$  in the  $z$ -direction.

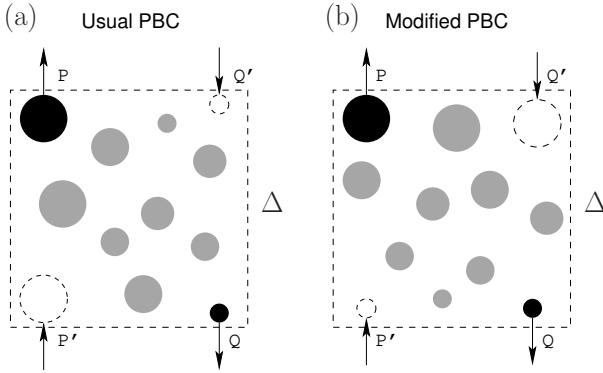


Fig. 4. (a) Under usual PBC a large droplet leaves the sampling box at some point  $P$  and is reintroduced into the box at  $P'$  with its radius unaltered. Accordingly, a small droplet that leaves the box at  $Q$  is reintroduced at  $Q'$  with the same radius. (b) The modified PBC shrinks the radius of a large droplet as it is reintroduced at  $P'$  after leaving the box at the point  $P$ . Accordingly, modified PBC expands the radius of a small droplet as it is reintroduced at  $Q'$  after leaving the box at the point  $Q$ .

cross the the bottom and top horizontal boundaries of the sampling volume. Usual and modified PBC are contrasted in Fig. 4. Imagine that a droplet leaves the sampling volume at the top boundary [point  $P$  in panels (a) and (b) of Fig. 4] with large squared radius. Under *usual* periodic boundary conditions the droplet will be reintroduced into the sampling volume at the bottom boundary (point  $P'$  of Fig. 4.a) with its large squared radius unaltered. However, due to the gradient  $\bar{\gamma}_a$ , the squared radius must be also adjusted when the droplet is reintroduced at point  $P'$  (as in Fig. 4.b) to produce a stable squared radius gradient over sufficiently long periods in the steady state. The modified PBC scheme is described in detail in Appendix A.

As for reflecting boundaries (Abade and Albuquerque 2024), modified PBC preserve the number of representative droplets in the ensemble. As an advantage, modified PBC can be (presumably) applied in DNS-like studies as well in the droplet-tracer limit (sedimentation and droplet inertia neglected). Also, modified PBC can be used to extract the fine-grained DSD due to deviations from the reversible condensation regime, as we shall discuss in Sec. 5.

Figure 3 shows that reflecting boundaries and the modified PBC are effective to enforce local sampling of the DSD and produce the same well-defined filtered variance  $\sigma_a(\Delta)$  for filter width  $\Delta$ .

### c. A reduced stochastic model

It follows from previous sections that the eddy hopping model builds up correlations between droplet sizes and droplet vertical positions. The resulting fine-grained DSDs are spatially inhomogeneous (along the vertical direction) and in general differ from the  $\Delta$ -dependent filtered DSD. It is then instructive to consider a simple model of

stochastic condensation [as the one discussed by Chandrakar et al. (2016) and Saito et al. (2019)] that coarsely represents DSD broadening in an idealized scenario, where the statistics of the droplet sizes is imagined to be spatially homogeneous. This scenario emerges in a certain type of DNS-like models of turbulent condensation that mimics an idealized homogeneous and unbounded cloud (to be discussed later in Sec. 6).

The reduced model comprises two equations, one for  $a$  and other for  $S$ ,

$$da = 2DSdt, \quad (20)$$

$$dS = -\frac{S}{\tau_s}dt + \sqrt{\frac{2\sigma_s^2}{\tau_s}}dW(t). \quad (21)$$

Unlike the eddy hopping model, the reduced model describes only two jointly distributed stochastic variables,  $a$  and  $S$ , regardless of the droplets positions and velocities. Also, the “noise” representing fluctuations enters directly in the Eq. (20) for supersaturation. Here, we assume the model parameters  $\sigma_s$  and  $\tau_s$  in Eq. (20) can be estimated. For the moment, we leave unspecified the physical processes that produce supersaturation fluctuations (and determine  $\sigma_s$  and  $\tau_s$ ).

It can be shown [see e.g., Chandrakar et al. (2016)] that this reduced model produces the same asymptotic continuous growth (18) of the variance of  $a$  (for  $t$  sufficiently longer than  $\tau_s$ ),

$$\sigma_a^2 = Kt, \quad t \gg \tau_s, \quad (22)$$

where  $K \equiv 8D^2\sigma_s^2\tau_s$ . However, if fluctuations in  $S$  are created by sources other than vertical velocity fluctuations, then the continuous growth of  $\sigma_a^2$  in (22) does not have the spatial interpretation as in (18) because  $a$  and  $S$  are decoupled from the droplet transport. The resulting fine-grained DSD is *spatially homogeneous* and thus coincides with the filtered DSD for arbitrary filter width  $\Delta$ .

The underlying sources of supersaturation fluctuations in the reduced model (as those due to vertical velocity fluctuations are excluded) may be stationary external boundary conditions that sustain the scalar fluctuations against turbulent mixing and scalar dissipation<sup>3</sup>. This external boundary condition determine the supersaturation variance  $\sigma_s^2$ , a model parameter. The other model parameter is  $\tau_s$ , the Lagrangian integral scale of  $S$  [Eq. (24)], which is difficult to measure in Lagrangian coordinates. Then  $\tau_s$  can be estimated by assuming the second-order Lagrangian structure function of  $S$ ,  $\langle dS^2(\tau) \rangle \equiv \langle [S(t+\tau) - S(t)]^2 \rangle$ , follows the

<sup>3</sup>In the Pi Chamber, stationary conditions at the top, bottom, and sidewalls determine how scalar fluctuations are maintained against turbulent mixing and scalar dissipation. Also, as the characteristic vertical displacement of air parcels in the Pi Chamber is a negligible fraction of the length scale  $1/A_1$ , different adiabatic cooling rates arising from turbulent fluctuations in the vertical velocities cannot be regarded as a source of variability in droplet growth conditions.



Kolmogorov scaling,

$$\langle dS^2(\tau) \rangle = C_1 \chi_s \tau, \quad (23)$$

where  $C_1$  is a constant,  $\chi_s$  is the mean dissipation rate of the scalar variance  $\langle S'^2 \rangle$ , and the time lag  $\tau$  lies in the inertial range (i.e.,  $\tau_\eta \ll \tau \ll \tau_s$ , where  $\tau_\eta$  is the Kolmogorov timescale). Relations of type (23) were thoroughly tested by Chandrakar et al. (2023) in high-resolution simulations of the Pi Chamber setup.

Then squaring Eq. (21), taking the ensemble average, and using (23) yield the amplitude  $\sqrt{C_1 \chi_s}$  ( $= \sqrt{2\sigma_s^2/\tau_s}$ ) of the random term in Eq. (21) and the time scale  $\tau_s = 2\sigma_s^2/(C_1 \chi_s)$ . The model parameters ( $\sigma_s, \tau_s$ ) here have no correlation with the statistics of droplets vertical velocities.

The four-equation eddy hopping model (Sec. 4) and the two-equation reduced stochastic model described above serve as prototypes of the two classes of DNS-like models we shall discuss later in Sec. 6.

#### d. The incomplete equivalence between reduced and eddy-hopping models

The scaling  $\sigma_a^2 \sim t$  [Eqs. (18) and (22)] for the variance is robust and will be observed in both eddy hopping and reduced stochastic models. As  $da/dt \propto S(t)$  (a linear relation) and  $S(t)$  is a stochastic process, then  $\sigma_a^2$  will eventually grow like  $t$  for times sufficiently longer than the supersaturation autocorrelation time  $\tau_s$ , defined as

$$\tau_s = \frac{1}{\sigma_s^2} \int_0^\infty R_s(t) dt, \quad (24)$$

where  $R_s(t) = \langle S'(t_0)S'(t_0+t) \rangle$  is the supersaturation autocorrelation function, with  $S' = S - \langle S \rangle$  and  $\sigma_s^2 = R_s(0)$ .

However, the essential point here is the *source* of the random fluctuations of  $S(t)$ . The DSD broadening described by the reduced model [Eqs. (20) and (21)] can be regarded as *strictly local* only if the noise in (21), which is parametrized by  $\sigma_s$  and  $\tau_s$ , is due to sources other than vertical velocity fluctuations. If the parametrization of supersaturation fluctuations include any source due to vertical velocity fluctuations, then this forcing will create correlations between droplets radii and droplet vertical positions. This implies that the fine-grained and filtered DSDs no longer coincide and the filtered DSD will depend on the filter width  $\Delta$ .

It has been suggested (Saito et al. 2021) that the two-equation model above [(20) and (21)] can be obtained by simplifying the eddy hopping model. Saito et al. (2021) showed that in the large scale limit, where the microphysics is fast compared to the slow turbulent mixing in large systems ( $\tau_{\text{ph}} \ll \tau_{\text{mix}} \sim \Delta^2/3$ ), the vertical velocity fluctuation  $w$  can be eliminated from the stochastic eddy hopping model. As shown by Saito et al. (2021), the statistical properties of supersaturation fluctuations in the simplified

model (namely,  $\sigma_s, R_s(t)$ , and thus  $\tau_s$ ) converge to those of the model without simplification as the ratio  $\tau_{\text{mix}}/\tau_{\text{ph}} \gg 1$  increases (i.e., as one approaches the large scale limit).

However, the elimination of  $w$  from the description masks the issues of non-local sampling discussed in Sec. 4.b. Also it removes the possibility of enforcing local sampling by using the approaches discussed in Sec. 4.b.

Moreover, although  $w$  is eliminated in the simplified model of Saito et al. (2021), vertical velocity fluctuations are the hidden source of supersaturation fluctuations as  $\sigma_w$  and  $\tau_w$  remain in the expressions for the parameters  $\sigma_s$  and  $\tau_s$  [see Eqs. (22) and (30) in Saito et al. (2021)]. At first sight, this procedure may suggest a ‘‘statistical equivalence’’ between the eddy-hopping model and its reduced version. However, this equivalence is incomplete, as the reduction procedure fixes only  $\sigma_s$  and  $R_s(t)$ , but hides correlations between droplets sizes and droplets vertical positions.

In an LES setting with particle-based microphysics, a proper implementation of the eddy hopping as an SGS microphysical model requires coupling between the vertical SGS droplet transport and the vertical velocity fluctuation  $w$  that drives the SGS supersaturation fluctuations, as we shall discuss in Sec. 7. Then the vertical velocity fluctuation should remain as an explicit model variable.

## 5. Deviations from the quasi-steady supersaturation

As discussed in Sec. 3, deviations from any of the three main assumptions [from (a) to (c)] underlying the reversible condensation scenario will work to destroy correlations between droplet size and droplet vertical position, creating conditions for strictly local broadening of the fine-grained DSD. The eddy hopping model incorporates two of these assumptions, namely, that all droplets in the ensemble experience the same supersaturation relaxation time  $\tau_s$  and that droplets follow the air flow as tracers (sedimentation and inertia are neglected). The eddy hopping model then allows for deviations from the quasi-steady supersaturation [Eq. (4)], being these deviations the only possible cause of broadening of the fine-grained DSD in the adiabatic (non-entraining) parcel framework.

In general, the supersaturation driven by vertical velocity fluctuations is frequency-dependent, that is, its response to fluctuations in the vertical velocity is retarded. This is clear after further inspection of Eqs. (12) and (15), which gives the linear relation

$$S(\omega) = \varphi(\omega)w(\omega), \quad \varphi(\omega) = \frac{A_1 \tau_s}{1 - i\omega \tau_s}, \quad (25)$$

between the Fourier-Laplace transforms  $S(\omega)$  and  $w(\omega)$  of  $S(t)$  and  $w(t)$ , respectively, where  $\omega$  is the frequency, and  $\varphi(\omega) = \varphi'(\omega) + i\varphi''(\omega) = |\varphi|e^{i\theta}$  is the amplitude- and

phase-modifying transfer function. The phase modification  $\theta = \arctan(\varphi''/\varphi')$  is due to the generally non-zero imaginary part  $\varphi''(\omega)$ . More details in Appendix B.

The quasi-steady approximation corresponds to the low-frequency limit  $\omega\tau_s \rightarrow 0$ , where  $S(\omega)$  and  $w(\omega)$  [and thus  $S_{qs}(\omega) \equiv A_1\tau_s w(\omega)$ ] are in phase (as  $\varphi''$  vanishes). For finite and high frequencies  $\omega\tau_s$ ,  $S(\omega)$  and  $w(\omega)$  are phase-shifted. Then the close link between supersaturation and vertical velocity is broken [see e.g., Khvorostyanov and Curry (1999)] and the condensation is no longer perfectly reversible (even when there is no variability in  $\tau_s$  among the droplets of the ensemble).

The quasi-steady approximation (4) cannot represent high-frequency supersaturation fluctuations. That is, fluctuations occurring on time scales shorter than the time constant  $\tau_s$  characterizing the relaxation of  $S$  to the quasi-steady value  $S_{qs}$  [Eq. (15)]. Associated with  $\tau_s$  there is a spatial lengthscale  $\ell_s$  (the supersaturation relaxation length). It can be estimated as (Kabanov et al. 1971; Clark and Hall 1979),

$$\ell_s \sim \varepsilon^{1/2} \tau_s^{3/2}, \quad (26)$$

where  $\varepsilon$  is the mean dissipation rate. The relation (26) is obtained on dimensional grounds by assuming that both  $\tau_s$  and  $\ell_s$  lie in the Kolmogorov's inertial range of cloud turbulence. This allows us to express the range of description supported by the quasi-steady approximation in terms of spatial lengthscales: the quasi-steady supersaturation fluctuation  $S_{qs}$  cannot represent microphysical variability due to vertical velocities of eddies of spatial scales smaller than  $\ell_s$ .

On short times compared to  $\tau_s$  (or small length scales compared to  $\ell_s$ ) the link between  $S$  and  $w$  is weaker and the condensation reversibility is broken [see e.g., Khvorostyanov and Curry (1999)]. This irreversibility allows  $w$  to generate supersaturation fluctuations  $S$  that may produce strictly local DSD broadening. These processes occurring on time scales  $\lesssim \tau_s$  and length scales  $\lesssim \ell_s$  are resolved (although coarsely represented) by the eddy hopping model if Eqs. (11) to (14) are numerically integrated using a short time step  $\delta t \ll \tau_s$ . This is shown in the scatterplots of  $z'$  and  $a'$  in Fig. 5.a for finite  $\tau_s$  and  $\ell_s$ , where a fine-grained DSD (red line) of finite breadth [measured by  $\sigma_a(0)$ ] can be observed. The fine-grained DSD in the steady state is however much narrower than the filtered DSD (gray line) for a filter width  $\Delta = 50$  m, as shown in Fig. 5.b.

Also, we may argue that inside a (generally small) volume of order  $\sim \ell_s^3$ , droplet sizes and droplet vertical positions are approximately uncorrelated. This feature has been noticed by Clark and Hall (1979) in the region of the activation layer, where the relaxation time  $\tau_s$  and its associated length scale  $\ell_s$  are enlarged compared to the conditions in the cloud core. As one advances towards the cloud core, inhomogeneities on scales larger than  $\ell_s$

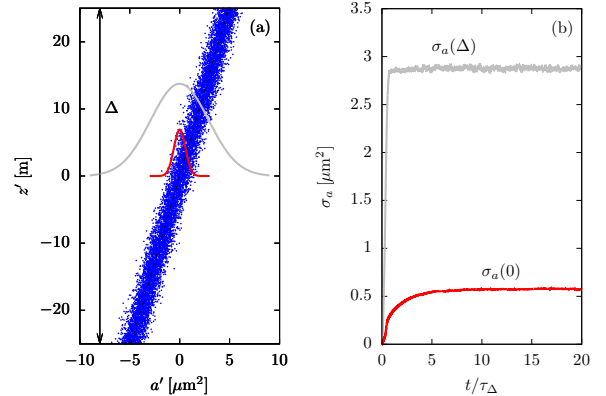


FIG. 5. Fine-grained versus filtered DSD for finite  $\tau_s$ . (a) Scatterplot of  $z'$  and  $a'$  (blue dots) along with the broad filtered DSD of filter width  $\Delta = 50$  m (gray line) and the much narrower fine grained DSD of vanishing filter width (red line); (b) time evolution of the filtered  $\sigma_a(\Delta)$  and fine-grained  $\sigma_a(0)$  standard deviation of  $a$ . Simulations using the eddy hopping model with modified PBC are for  $N = 100 \text{ cm}^{-3}$ ,  $\varepsilon = 10^{-3} \text{ m}^2 \text{ s}^{-3}$ ,  $\Delta = 50 \text{ m}$ ,  $\langle S \rangle = 0$ , and  $\langle a \rangle = a_0 = 100 \mu\text{m}^2$ . The scale height is  $H_a \approx 3 \text{ m}$  in the steady-state.

dominate and the regime of (large-scale) nearly reversible condensation is restored. Figure 6 shows the increase of the breadth  $\sigma_a(0)$  of the fine-grained DSD with  $\tau_s$  (and  $\ell_s$ ). The time constant  $\tau_s$  and the corresponding length  $\ell_s$  were changed by considering different droplet number concentrations  $N$  as indicated in Fig. 6. Thus in a scenario where supersaturation fluctuations  $S$  (and the resulting variability in droplet growth conditions) arises from turbulent vertical velocity fluctuations only, effective local broadening of the fine-grained DSD can emerge.

Finally, we note that an alternative picture can be provided by examining the power spectrum  $E_S(\omega)$  of the supersaturation fluctuation  $S(t)$  driven by vertical velocity fluctuations  $w(t)$ . In Appendix B we derive the expression for  $E_S(\omega)$  predicted by the eddy hopping model.

Figure 7 shows the dimensionless spectrum  $\hat{E}_S(\hat{\omega})$  [Eq. (B3)] as a function of the dimensionless frequency  $\hat{\omega} = \omega\tau_s$  for different values of  $\alpha = \tau_s/\tau_w$ , the ratio of the integral time scales of  $S(t)$  and  $w(t)$ . As  $\tau_s = 1/(\tau_{ph}^{-1} + \tau_{mix}^{-1}) \approx \min\{\tau_{ph}, \tau_{mix}\}$  and  $\tau_{mix} \approx \tau_w$ , the parameter  $\alpha$  is closely related to the inverse of the Damköhler number  $Da$ , defined as  $Da \equiv \tau_{mix}/\tau_{ph}$ . It is clear from Fig. 7 that the major contribution to the variance  $\sigma_S^2 = \int_0^\infty E_S(\omega) d\omega$ , and hence to the variance  $\sigma_a^2$  of droplet squared radius, comes from the lower frequency range. As the ratio  $\alpha = \tau_s/\tau_w$  increases ( $Da$  decreases), this frequency range shifts towards larger frequencies.

The high-frequency cutoff  $\omega_c$  (defined so that  $\int_0^{\omega_c} E_S(\omega) d\omega$  approximates  $\sigma_S^2$  well enough) is specified by the time step  $\delta t$  used to integrate the stochastic eddy-hopping model equations (11)-(14) numerically. This time

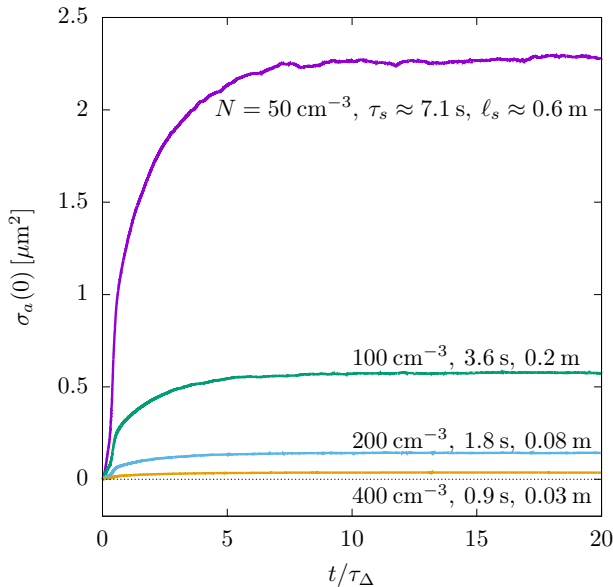


FIG. 6. Fine-grained  $\sigma_a(0)$  for different droplet number concentrations  $N$  (the corresponding  $\tau_s$  and  $\ell_s$  in the steady state are also indicated). Larger  $\tau_s$  (and  $\ell_s$ ) leads to broader fine-grained DSD. Simulation parameters are the same as in Fig. 5, except for  $N$ .

step should satisfy the condition  $\delta t \ll \tau_s$ . In the so-called DNS-like models of type A (to be discussed in Sec. 6),  $\omega_c$  is specified by the spatial resolution  $\delta x$  of the computational grid. Accordingly, the spatial resolution should be fine enough to satisfy the condition  $\delta x \ll \ell_s$  (Clark and Hall 1979). Figure 7 suggests that the high-frequency cutoff  $\omega_c$  increases as  $\alpha$  increases (Da decreases).

## 6. DNS-like studies

Direct numerical simulations (DNS) studies<sup>4</sup> of turbulent condensation may be separated into two types based on how supersaturation fluctuations are created:

- (A) by local vertical velocity fluctuations via the adiabatic cooling effect, or
- (B) by random forcing of the thermodynamic scalars (temperature  $T$  and vapor mixing ratio  $q$ , or supersaturation  $S$ ) applied isotropically on the large scales of the computational box of size  $\Delta$ .

Appendix C summarizes the equations comprising the DNS models of type A and B. They resolve the velocity and thermodynamic scalar fields more faithfully than the simple stochastic models described in Sec. 4. However, the eddy-hopping and the reduced models serve as useful prototypes of DNS models of type A and B, respectively.

<sup>4</sup>Here and henceforth DNS actually means “DNS-like” studies as they also include the so-called scaled-up DNS of (Thomas et al. 2020) and implicit large eddy simulations (ILES) studies of Grabowski and Thomas (2021) and Grabowski et al. (2022b,a).

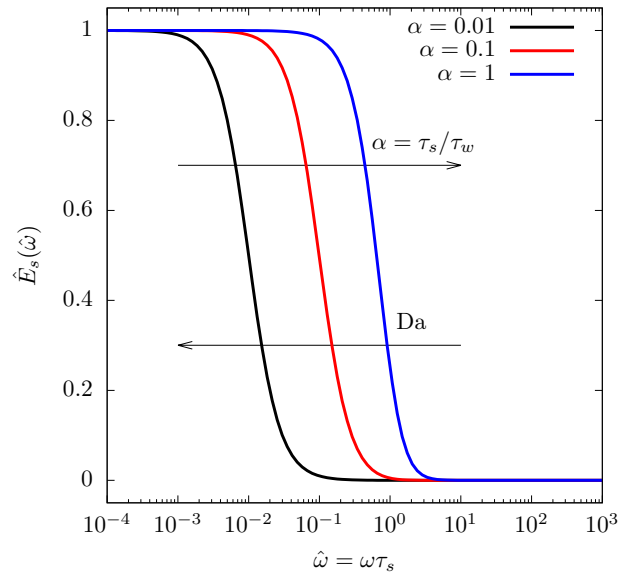


FIG. 7. Dimensionless power spectrum  $\hat{E}_s(\hat{\omega})$  of supersaturation fluctuations as a function of the dimensionless frequency  $\hat{\omega} = \omega\tau_s$  for different values of the parameter  $\alpha = \tau_s/\tau_w$ . The arrow to the left indicates the direction of increasing Damköhler number  $Da \equiv \tau_{\text{mix}}/\tau_{\text{ph}}$ .

### a. DNS-like models of type B

DNS studies of type B neglect the adiabatic cooling effect and simulate supersaturation fluctuations solely produced by the scalar forcing at large scales  $\sim \Delta$ . This scalar forcing mimics the effects of external boundary conditions that sustain scalar fluctuations against turbulent mixing. The works by Paoli and Shariff (2009), Siewert et al. (2017) and Saito et al. (2019) belong to this type of DNS studies, which actually model turbulent condensation in an unbounded and homogeneous cloud. General features of DNS models of type B can be understood by analyzing the reduced stochastic model discussed in Sec. 4.c, provided  $\sigma_s^2$  is due to sources other than vertical velocity fluctuations.

DNS models of type B produce polydisperse droplet dispersions with spatially homogeneous droplet size statistics as does the reduced stochastic model of Sec. 4.c. In this scenario, usual periodic boundary conditions (PBC) in all directions are applicable to mimic an unbounded system, where cloud boundaries are imagined to be removed to infinity. The fine-grained DSDs coincide with filtered DSDs (for arbitrary filter width) and these models are thus free from artifacts that could mask the real origin of the observed local DSD broadening. This is not the case of DNS model of type A, as we shall discuss below.

### b. DNS-like models of type A

DNS studies of type A do not apply any large-scale scalar forcing, but rely on the local adiabatic cooling effect (driven

by vertical velocity fluctuations) as the only source of supersaturation variability. Their purpose is to confine the problem of turbulent condensation to a study of the effect of “local” or “internal” sources of thermodynamic variability caused by velocity fluctuations on a range of length scales smaller or of the order of  $\Delta$ . The works by Celani et al. (2005, 2008, 2009); Lanotte et al. (2009); Sardina et al. (2015, 2018); Saito and Gotoh (2018); Thomas et al. (2020); Grabowski and Thomas (2021); Grabowski et al. (2022b,a) belong to this rather problematic class of DNS models.

DNS models of type A give rise to polydisperse droplet dispersions with droplet size statistics that is spatially inhomogeneous in the vertical direction as in the stochastic eddy hopping model. In this case, the periodic computational box containing the droplets should be regarded as a small sample embedded in a cloud which has a mean squared radius gradient in the vertical direction (Sec. 4.b). Despite being ill-suited for this scenario, usual PBC (Fig. 4.a) in the vertical direction have been the rule in DNS models of type A, thus causing numerical artifacts.

Issues with DNS studies of this type were generally suggested by Prabhakaran et al. (2022). Their argument was formulated in terms of “inadequate representation of vertical turbulent transport” and on the fact that “all the cloud droplets have the same life time” in these idealized frameworks. Here we refine the statements of Prabhakaran et al. (2022) and explain in more detail the sources of the numerical artifacts in DNS models of type A.

### c. Artifacts in DNS models of type A

The problem with DNS studies of type A arises from misuse of PBC in the direction (vertical) along which the statistics of droplet sizes is spatially inhomogeneous. Usual PBC (illustrated in Fig. 4.a) takes a cloud droplet that had left the computational box, say, through the top, and puts it back at the bottom of the domain (keeping the droplet size). If these droplets trajectories (corrected by usual PBC) were “unfolded”, then it would reveal that droplets actually diffuse in the vertical due to turbulent fluctuations. Thus the actual averaging length scale  $\tilde{\Delta}$  grows beyond the computational box size  $\Delta$  (where momentum forcing is applied) and follows the scaling  $\sim t^{1/2}$  as in the eddy hopping model operating in adiabatic parcels (see Sec. 4 and illustrated in Fig. 2.a.<sup>5</sup>

Alternatively, the issue can be understood in the reversible condensation scenario, which emerges on the large

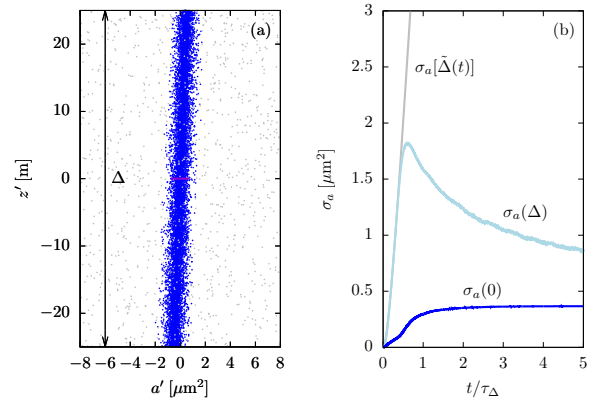


FIG. 8. (a) Scatterplot of  $a'$  and  $z'$  using usual PBC (gray dots) and modified PBC (blue dots) for a background average supersaturation  $\langle S \rangle = 0.01$ . Usual PBC artificially decorrelates  $a'$  and  $z'$  by mixing small and large droplets in the computational box. (b) Time evolution of the standard deviations  $\sigma_a[\tilde{\Delta}(t)]$  (usual PBC),  $\sigma_a(\Delta)$  and  $\sigma_a(0)$  (corresponding to the filtered and fine-grained DSDs obtained under modified PBC). The results were obtained by numerical integration of the eddy-hopping model equations (a prototype for DNS-like models of type A). The scale height [Eq. (10)] is  $H_a \approx 7$  m at  $t/\tau_\Delta = 5$  and reaches  $H_a \approx 18$  m in the quasi-steady state.

scales ( $\gg \ell_s$ ) inside the DNS computational box. We argue that the usual PBC, which returns a large droplet (that had left the computational box at the top) back to the bottom of the domain (and keeps its large radius), artificially brakes the large-scale near reversibility of the condensation. It enforces that large and small droplets coexist in the computational box of characteristic size  $\Delta$  and incorrectly predicts DSD continuous broadening, which cannot be regarded as “local”. This is shown in Fig. 8. The gray dots in Fig. 8.a show that usual PBC decorrelates  $a$  and  $z$  by vertically mixing small and large droplets in the computational box. The corresponding breadth  $\sigma_a[\tilde{\Delta}(t)]$  grows continuously in time (Fig. 8.b). Conversely, modified PBC preserves the vertical gradient of the droplet squares radius (blue dots in Fig. 8.a). The breadths  $\sigma_a(\Delta)$  and  $\sigma_a(0)$  of the corresponding filtered and fine-grained DSDs reach quasi-stationary values with  $\sigma_a(\Delta) > \sigma_a(0)$  (Fig. 8).

Also, usual PBC in DNS models of type A vertically mixes large and small droplets and creates spurious spatial correlations between droplets of different sized at short separations. This may artificially enhance droplet collision probabilities, which is essential for the onset of collision-coalescence. We shall discuss this further in Sec. 7.c. For instance, the observation in DNS data by (Celani et al. 2005) that small and large droplets cohabit in small volumes (and that it may enhance droplet collision probabilities) might have been distorted by the artificial effects of usual PBC.

Finally, we note that besides using modified PBC we have to use sufficiently high grid resolutions to properly

<sup>5</sup>Note that models producing local fluctuations in  $T$  (or  $S$ ) by fluctuations in  $w$  via the adiabatic cooling effect implicitly assume that air parcels ascending in the computational box expand due to the vertical decrease of the base-state hydrostatic pressure. This vertical gradient in the base-state pressure evidently brakes the translational invariance within the DNS computational box. This inhomogeneity is absent in DNS studies of type B.

predict fine-grained DSDs and the spatial correlations between “large” and “small” droplets. The analysis of Clark and Hall (1979) and our discussion in Sec. 5 suggest that actual local DSD broadening can be observed only on small length scales compared to the supersaturation relaxation length scale  $\ell_s$ . Then the DNS grid needs to resolve small scales  $\lesssim \ell_s$ , as anticipated by Clark and Hall (1979). The local broadening arising from the irreversible coupling between supersaturation fluctuations and the vertical motion of air parcels is expected to be enhanced around the activation layer (larger  $\tau_s$  and  $\ell_s$ ) and suppressed under cloud core conditions (smaller  $\tau_s$  and  $\ell_s$ ) as indicated in Fig. 6.

#### d. Sedimentation and droplet inertia

Another important question is the treatment of droplet transport by the turbulent flow. If we assume the droplets follow the turbulent air flow  $\mathbf{u}(\mathbf{x}, t)$  — the droplet-tracer limit —, thus the droplet trajectory  $\mathbf{X}$  is defined via  $\partial_t \mathbf{X} = \mathbf{u}[\mathbf{X}(t), t]$ . Otherwise, if we cannot neglect the effects of droplet inertia (characterized by the Stokes number  $St$ ) and sedimentation (characterized by the settling number  $Sv$ ), then  $\mathbf{X}(t)$  is determined via

$$\partial_t \mathbf{X} = \mathbf{u}[\mathbf{X}(t), t] + \text{corrections}(St, Sv), \quad (27)$$

where the corrections to the droplet-tracer limit depend on the Stokes and settling numbers.

In DNS studies of type A that additionally assume the droplet-tracer limit (as the eddy hopping model), the microphysics is maximally coupled with the droplet transport (the positive correlation between droplets sizes and their vertical positions is maximized). As written, ill-suited usual PBC in the vertical direction artificially and thus unphysically brakes this correlation. Droplet inertia and sedimentation work to weaken the correlation between microphysics and droplet transport in the scenario of  $w$ -driven microphysical variability. However, DNS studies that solve an equation like (27) for the droplet transport [e.g., Lantotte et al. (2009); Celani et al. (2005)] have considered mainly regimes of small  $St$  and  $Sv$ , where the so-called crossing-trajectory effects arising from sedimentation and droplet inertia are negligible.

## 7. Eddy hopping as a subgrid scheme in LES

If used as an SGS condensation scheme in LES with particle-based microphysics, the eddy hopping model will predict filtered DSD that tend to be broader than the those prognosed under the uniform condensation approximation, where all droplets in a particular grid box experience the same filtered (grid-averaged) supersaturation  $\langle S \rangle$ . This has some implications that we shall discuss here.

First, to prevent the eddy hopping model from predicting artificial DSD broadening (through the non-local sampling discussed for the adiabatic cloud parcel), the SGS

turbulent transport of cloud droplets must be treated properly. Second, if the SGS scheme predicts a broader filtered DSD, then this will certainly have an impact on the filtered condensation rate, and hence on the filtered buoyancy production. Finally, broader filtered DSDs may (at least in principle) indicate enhanced probabilities of collision-coalescence of droplets due to differential sedimentation. However, enhancement of collision probabilities actually occurs only if the physics underlying the SGS scheme is able to produce strictly local DSD broadening, which manifests itself mainly in the fine-grained DSD and not only in the filtered DSD.

#### a. SGS droplet transport

If the eddy hopping model is used as a subgrid scheme in LES, then it must provide microphysical properties that refer to a particular grid box of size  $\Delta$ , and hence, these properties must be sampled over a local averaging volume of characteristic size  $\Delta$ . (Here we assume for simplicity that the computational grid is isotropic with the same spatial resolution  $\Delta$  in all directions.) To enforce this *local sampling* in LES, the SGS vertical transport of droplets must be driven by the same SGS velocity fluctuations  $w$  driving SGS supersaturation fluctuations  $S$ .

Otherwise, if the SGS model for condensation (including fluctuations in  $S$  driven by  $w$ ) is decoupled from the SGS droplet transport, then it will spuriously overestimate the local width of the filtered DSD. For example, this is the risk we run while implementing in LES an SGS scheme like the simplified stochastic model suggested by Saito et al. (2021) (see Sec. 4.d), where the SGS vertical velocity fluctuation  $w$  no longer appears as a resolved model variable (although its underlying effects are parametrized in the simplified model).

Even when the droplet SGS transport is properly treated, the local variance of the filtered DSD may depend on the grid resolution  $\Delta$  (the filter width) if it is larger or of the same order of  $H_a$ .

In an LES setting,  $w$  is the vertical component of the unresolved fluid velocity  $\mathbf{u}$ ,  $w = \hat{\mathbf{e}}_z \cdot \mathbf{u}$ . The velocity fluctuation  $\mathbf{u}$  can be modeled by a stochastic differential equation of the form [see e.g., Pope (1994)]

$$d\mathbf{u} = \alpha dt - \frac{\mathbf{u}}{\tau_u} dt + \sqrt{\frac{2\sigma_u^2}{\tau_u}} d\mathbf{W}(t), \quad (28)$$

where  $d\mathbf{W}(t)$  is the increment of an isotropic vector-valued Wiener process. Equation (28) applies for the general case of inhomogeneous turbulent flow in cloud scale simulations. It differs from (13), which is for idealized adiabatic parcels filled with homogeneous turbulence, by the drift term [see e.g., MacInnes and Bracco (1992)],

$$\alpha = \nabla \cdot \langle \mathbf{u}\mathbf{u} \rangle - \mathbf{u} \cdot \nabla \langle \mathbf{u} \rangle, \quad (29)$$

where  $\langle \mathbf{U} \rangle$  is the filtered velocity field resolved by the dynamical core of the cloud LES scheme, and  $\langle \mathbf{u}\mathbf{u} \rangle$  is the kinematic Reynolds stress tensor. (Here, the spatial filtering operation denoted by  $\langle \cdot \rangle$  is the same defined in (2) for the DSD and consider filter width equal to the LES resolution length  $\Delta$ .) Also,  $\tau_w$  in Eq. (13) for stationary homogeneous turbulence is an integral timescale, while  $\tau_u$  in (28) for inhomogeneous turbulence represents a local velocity decorrelation timescale [see e.g., Rodean (1996); Pope (2011)]. In the droplet-tracer regime the droplet position  $\mathbf{X}$  is determined by integrating the SDE  $d\mathbf{X} = [\langle \mathbf{U} \rangle + \mathbf{u}]dt$ . Equations (28) and (29) constitute the simplified Langevin model (SLM) for the fluid particle velocity fluctuation used in several applications [see e.g., Pope (1994); MacInnes and Bracco (1992)].

A scheme that couples  $w$  driving supersaturation fluctuations and vertical SGS droplet transport was recently implemented in cloud scale simulations by Chandrakar et al. (2021). They use an expression derived by Weil et al. (2004) for the drift term  $\alpha$ , which is an approximation to Eq. (29). Although (29) is essentially “kinematic” (i.e., it arises as a kinematic step while writing the equation of motion for the fluctuation  $\mathbf{u}$  from the NS equations for the full velocity  $\mathbf{U} = \langle \mathbf{U} \rangle + \mathbf{u}$ ), the approximated drift term used by Weil et al. (2004) and Chandrakar et al. (2021) makes this feature less transparent. Also, Chandrakar et al. (2021) included an additional random forcing to the stochastic equation for the SGS Lagrangian supersaturation fluctuation, parametrized by a prescribed supersaturation standard deviation  $\sigma_s$ . Although Chandrakar et al. (2021) argue that this additional forcing arises from sources other than vertical velocity fluctuations, they specify  $\sigma_s$  in terms of the velocity fluctuation parameters  $\sigma_u$  and  $\tau_u$ . A more physically appealing route to parametrize this stochastic forcing term of supersaturation fluctuations has been considered in Chandrakar et al. (2023) as we discussed in Sec. 4.c.

Finally, we briefly remark on the Lagrangian cloud model L3 by Hoffmann et al. (2019) and Hoffmann and Feingold (2019). In this model, the SGS droplet transport is not linked to the SGS vertical velocity fluctuations that partially contribute to the subgrid microphysical variability (through differential adiabatic cooling rates experienced by the cloud droplets). The L3 model combines an LES dynamical core with a particle-based microphysics, where the so-called linear eddy model (LEM) [see e.g., Kerstein (1988); Krueger et al. (1997)] is used to represent SGS turbulent mixing of the thermodynamic scalars. LEM solves the molecular diffusion of scalars on a one-dimensional grid (the LEM grid), which is periodically rearranged and compressed (using the so-called triple map) to simulate turbulent advection. As stated by Hoffmann et al. (2019) and Hoffmann and Feingold (2019), LEM also accounts for the SGS microphysical variability arising from variability of adiabatic cooling rates experienced by different droplets in a given LES grid box. This arises from stochastic vertical

motions due to the LEM triplet map, because the droplets experience the same rearrangements as the boxes of the LEM grid, which is aligned vertically. However, the actual SGS vertical droplet transport (which is due to stochastic velocities computed from the SGS turbulent kinetic energy  $k$ ) and the stochastic vertical motions of the LEM grid boxes (due to the LEM triplet map) are apparently uncorrelated.

### b. Grid-averaged condensation rate

In an LES setting of spatial resolution  $\Delta$ , the balance equation for the filtered vapor mixing ratio  $\langle q \rangle$  has the form

$$\partial_t \langle q \rangle = -\langle C \rangle + \dots, \quad (30)$$

where  $\langle C \rangle$  is the spatially filtered (or grid-averaged) condensation rate. (Again, the spatial filtering  $\langle \cdot \rangle$  is the same as in (2) for the DSD.) The dots on the RHS of (30) denote other contributions to local changes in  $\langle q \rangle$ , such as advection by the turbulent flow and molecular diffusion of water vapor.

In particle-based schemes [see e.g., Shima et al. (2009); Arabas et al. (2015); Dziekan et al. (2019); Hoffmann et al. (2019)], the filtered condensation rate is calculated directly. If we neglect for simplicity surface tension and solute effects and assume each droplet grows according to (3), then  $\langle C \rangle$  may be approximated as

$$\langle C \rangle \approx \alpha \sum_k r_k S_k, \quad \alpha = \frac{4\pi\rho_w D}{\rho_d V_\Delta}, \quad (31)$$

where the sum is over all cloud droplets in the grid box of volume  $V_\Delta$ ,  $r_k$  is the radius of the  $k$ th droplet experiencing a supersaturation  $S_k$ ;  $\rho_w$  and  $\rho_d$  are the densities of water and dry air, respectively. Also, we assume that the effective vapor diffusion coefficient  $D$  varies weakly in  $V_\Delta$ .

By decomposing

$$r_k = \langle r \rangle + r'_k, \quad S_k = \langle S \rangle + S'_k, \quad (32)$$

where  $\langle \cdot \rangle$  denotes averages over all droplets in  $V_\Delta$  at a particular time, we may write

$$\langle C \rangle = \alpha N [\langle r \rangle \langle S \rangle + \langle r' S' \rangle], \quad (33)$$

where  $N$  is the total droplet concentration in the grid box. Thus the condensation rate  $\approx \alpha N \langle r \rangle \langle S \rangle$  under the uniform condensation approximation is increased by a factor proportional to the covariance  $\langle r' S' \rangle$  if this is positive. For collisionless and non-sedimenting droplets, a positive correlation between  $S$  and  $r$  simply indicates that the large droplet tail of the filtered DSD is formed by those droplets that experienced higher supersaturation along their growth histories.



An equation like (33) was considered by Paoli and Shariff (2009). They stated that the *closure problem* of determining the filtered condensation term  $\langle C \rangle$  boils down to modeling the covariance  $\langle r'S' \rangle$  (i.e., writing it in terms of model resolved variables). The eddy hopping model used as a particle-based SGS scheme provides a “closure” by explicitly calculating  $\langle C \rangle$  beyond the uniform condensation approximation. The resulting broadening of the filtered DSD predicted by the eddy hopping model renders  $\langle r'S' \rangle > 0$  and leads to increased local condensation rates compared with those obtained under uniform condensation. Enhanced filtered condensation rates does not require locally broader fine-grained DSDs; broader filtered DSDs suffice. In contrast, enhanced droplet collision probabilities are supported by broader fine-grained DSDs only, as we shall discuss next.

### c. Stochastic droplet coalescence

Although we are primarily focused on the DSD formed by the growth of collisionless droplets through condensation, the resulting DSD impacts the onset of gravity-induced droplet collision-coalescence.

Particle-based schemes for cloud microphysics, such as the superdroplet method (SDM) developed by Shima et al. (2009), treat droplet collision-coalescence in a probabilistic manner through a Monte Carlo method. This requires the probability  $P_{ij}$  that two droplets (labeled  $i$  and  $j$ ) will coalesce inside a volume  $V$  during the time interval  $(t, t + \delta t)$ . This probability is given by

$$P_{ij} = K_{ij} \delta t / V, \quad (34)$$

where  $K_{ij}$  is the coalescence kernel. For droplet collisions induced by gravity through differential sedimentation,

$$K_{ij} \propto (r_i + r_j)^2 |w_{\text{sed}}(r_i) - w_{\text{sed}}(r_j)|, \quad (35)$$

where  $w_{\text{sed}}(r)$  is a parametrization for the sedimentation velocity of a droplet of radius  $r$ .

An essential assumption underlying (35) is that the colliding droplets are well-mixed inside  $V$  [see e.g., Gillespie (1972); Shima et al. (2009); Dziekan and Pawlowska (2017)] as spatial correlations between droplets is not parametrized in the collision kernel (35)<sup>6</sup>. In an LES setting, it is generally assumed that the volume  $V$  in (34) is associated with the model spatial resolution, hence with the

<sup>6</sup>Consider a “small” droplet of radius, say,  $r_s = \langle r \rangle_\Delta - 2\sigma_r(\Delta)$  and a “large” one of radius  $r_l = \langle r \rangle_\Delta + 2\sigma_r(\Delta)$  are located at the same grid box of size  $\Delta$ , where the average radius  $\langle r \rangle_\Delta$  and the standard deviation  $\sigma_r(\Delta)$  refer to the filtered DSD  $\langle n(r) \rangle_\Delta$ . Now assume  $N_l$  is the number concentration of large droplets. We define the radial distribution function  $g_{sl}$  for small and large droplets such that  $N_l g_{sl}(\mathbf{x}) d\mathbf{x}$  is the (ensemble) average number of large droplets in a volume element  $d\mathbf{x}$  at the position  $\mathbf{x}$  from a small droplet. The gravity collision kernel (35) assumes  $g_{sl}(d\hat{\mathbf{x}}) = 1$ , where  $d = r_s + r_l$  and  $\hat{\mathbf{x}} = \mathbf{x}/|\mathbf{x}|$ , while in fact  $g_{sl}(d\hat{\mathbf{x}}) \approx 0$ .

volume  $V_\Delta$  of the computational grid box. Compared with the uniform condensation approximation, the eddy hopping model used as an SGS condensation scheme tends to predict relatively broad filtered DSD (of underlying sampling volume  $\sim V_\Delta$ ). However, large and small droplets forming the left and right tails of the predicted filtered DSD might not be well-mixed in the volume  $V_\Delta$  of the grid box. This is illustrated by scatterplots of  $a$  and  $z$  in Fig. 9. In fact, at the early stages of condensation, large and small droplets may be well separated in the computational grid box (as sedimentation is still too slow to effectively mix large and small droplets). This may lead to conceptual difficulties in calculating collision probabilities according to (35).

As discussed in Sec. 5, the eddy hopping model (relying on  $S$  driven solely by  $w$ ) presumably produces droplet size statistics that are spatially homogeneous only on scales smaller or of the order of the supersaturation relaxation length scale  $\ell_s$ . Then one may argue that the well-mixed volume  $V$  has a characteristic linear size  $V^{1/3} \lesssim \ell_s$ , which may be much smaller (e.g., under cloud core conditions) than the volume  $V_\Delta$  of the computational grid boxes. Also,  $\langle n(r) \rangle_{\ell_s}$  (the filtered DSD with filter width  $\sim \ell_s$ ) is much narrower than  $\langle n(r) \rangle_\Delta$  (the filtered DSD with filter width  $\sim \Delta$ ). Thus droplet collision probabilities in  $V \sim \ell_s^3$  may not be significantly enhanced (at least in the cloud core) under the turbulent condensation represented by the eddy hopping model. Figure 9.b shows how the dispersion  $\sigma_{z|a}$  around the expected height  $\langle z|a \rangle$  of a droplet of squared radius  $a$  depends on  $\ell_s$ . As  $\ell_s$  increases, the heights of a “small” and a “large” droplet are more broadly distributed, thus enhancing the probability of finding droplets of different sizes close to each other.

## 8. Conclusions

In this paper we discussed that any turbulent condensation model that (in some degree) relates supersaturation fluctuations  $S$  experienced by cloud droplets with their vertical velocity fluctuations  $w$  will produce correlations between droplet sizes and droplet vertical positions in a cloudy volume. As a consequence, the statistics of droplet sizes produced by such a model will be spatially inhomogeneous along the vertical direction. This implies that the droplet size distribution (DSD) will depend on the spatial scale over which the distribution is sampled. To systematically discuss this dependence on the sampling spatial scale, we have defined (Sec. 2) the fine-grained DSD  $n(r)$  and the filtered DSD  $\langle n(r) \rangle_\Delta$  of filter width  $\Delta$ . Thus when the droplet size statistics is spatially inhomogeneous, then fine-grained DSDs that are locally narrow may render filtered DSDs that are locally broad in a discretized domain of spatial resolution  $\Delta$  if  $\Delta$  is sufficiently large compared to  $H_a$  [Eq. (10)].

A simple model that links  $S$  with  $w$  is the stochastic eddy hopping model (Sardina et al. 2015; Grabowski and

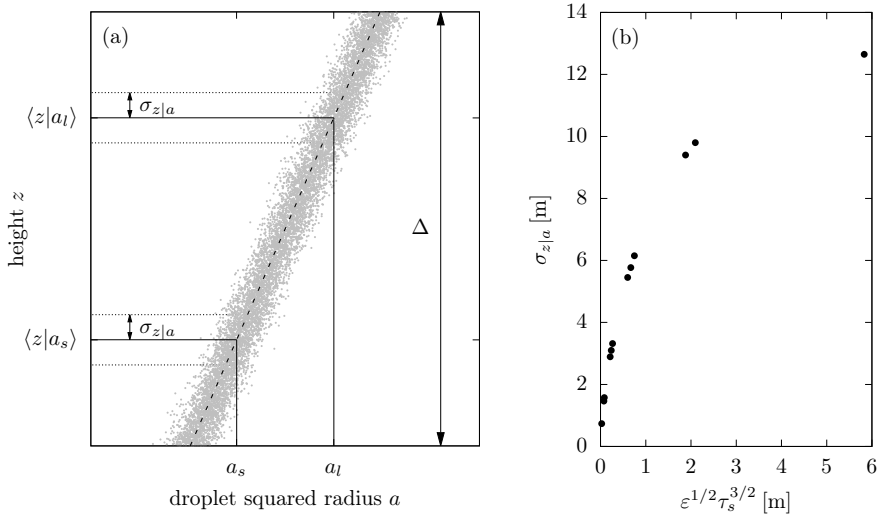


FIG. 9. (a) Scatterplot of  $a$  and  $z$  showing the conditional expected heights  $\langle z|a_s \rangle$  and  $\langle z|a_l \rangle$ , respectively, of a “small” droplet (of squared radius  $a_s$ ) and a “large” droplet ( $a_l$ ). Considering the indicated conditional dispersion  $\sigma_{z|a}$  in heights, these “large” and “small” droplets are in fact well-separated (and *not* thoroughly mixed) in the volume of characteristic length  $\Delta$ . (b) Conditional standard deviation  $\sigma_{z|a}$  of heights (for a given  $a$ ) as a function of the supersaturation length scale  $\ell_s \sim \varepsilon^{1/2} \tau_s^{3/2}$ . The points are for  $\varepsilon$  in the range  $0.001 - 0.1 \text{ m}^2 \text{ s}^{-3}$  and droplet number concentration  $N$  in the range  $50 - 400 \text{ cm}^{-3}$ .

Abade 2017; Abade et al. 2018), where vertical velocity fluctuations causes supersaturation variability through the adiabatic cooling effect. The idea behind the eddy hopping model is that, in a relatively large cloudy volume (say, of the size of a typical LES grid box), various cloud droplets (that are representative of the whole droplet population in this large cloudy volume) may experience different adiabatic cooling rates depending on the vertical turbulent velocity of the air carrying these droplets.

Used as a stand-alone representation of turbulent condensation in adiabatic parcel framework, the original version of the eddy hopping model produces broadening of the parcel DSD that continuously grow in time. We have shown that this continuous growth does not reflect an actual local DSD broadening [as supposed by Sardina et al. (2015); Grabowski and Abade (2017); Abade et al. (2018)], but arises from the “non-local” sampling caused by the growth with time (like  $\sim t^{1/2}$ ) of the spatial scale (or filter width) associated with the sampling volume containing the whole droplet population of the parcel. The sampling volume is implicitly related to the spatial extent of the droplet turbulent diffusion in the vertical direction, which is driven by the same vertical velocity fluctuations that cause variability in the supersaturation experienced by different droplets. To enforce local sampling in the adiabatic parcel framework, we considered (Sec. 4.b) alternative boundary conditions (reflecting and modified PBC) at the top and bottom horizontal boundaries of the sampling volume (see Sec. b).

A certain type of DNS-like models of turbulent condensation [e.g., Celani et al. (2005, 2008, 2009); Lanotte

et al. (2009); Sardina et al. (2015, 2018); Saito and Gotoh (2018); Thomas et al. (2020); Grabowski and Thomas (2021); Grabowski et al. (2022b,a)], as they create supersaturation fluctuations through local vertical velocity fluctuations, has the same artifacts as the much simpler stochastic eddy hopping model. Hence the broad DSD these DNS-like studies predict cannot be regarded as strictly local. Free of such inconsistencies are other DNS studies [e.g., Paoli and Shariff (2009); Siewert et al. (2017); Saito et al. (2019)], where supersaturation fluctuations are sustained by random scalar forcing applied on the largest scales of the computational box (supersaturation fluctuations at small scales are determined by downscale nonlinear transfer).

The eddy hopping model can be used as a subgrid condensation scheme in LES (with particle-based microphysics) and tends to predict broad filtered DSD relative to the uniform condensation approximation. We emphasized in this work that actual local sampling of the filtered DSD must be enforced in LES by properly coupling the subgrid droplet transport with the subgrid vertical velocity fluctuations that cause subgrid supersaturation fluctuations.

Broader filtered DSD predicted by the eddy hopping model may increase local (grid-averaged) condensation rates in LES compared with uniform condensation. However, broad filtered DSD does not necessarily imply enhanced probabilities of droplet collisions induced by differential sedimentation (as broad filtered DSD does not imply broad fine-grained DSD). Broader fine-grained DSD can be supported by the eddy hopping model only through the condensation reversibility breaking that may occur at



small scales of the order of the supersaturation relaxation lengthscale  $\ell_s$  [see Sec. 5 and the analysis of Clark and Hall (1979)]. However, the filtered DSD  $\langle n(r) \rangle_{\ell_s}$  with filter width  $\sim \ell_s$  may be narrow in the cloud core (under the turbulent condensation represented by the eddy hopping model) and cannot effectively enhance droplet collision probabilities.

The analysis presented in this paper neglects the effects of droplet inertia and sedimentation. As these effects deviate droplets from Lagrangian fluid trajectories, droplet inertia and sedimentation affect the Lagrangian correlation time  $\tau_s$  for the supersaturation fluctuations and work to destroy correlations between droplet sizes and droplet vertical positions. Clarifying these effects poses several challenges to stochastic representations of turbulent condensation, such as the eddy hopping model. However, this problem can be tackled by DNS-like models, as done, for instance, by Vaillancourt et al. (2002).

It should be evident that the eddy hopping model (and the DNS-like models where  $S$  is driven by  $w$ ) cannot explain the stationary DSD obtained from simulation data of the Pi Chamber setup, as those reported and analyzed by Prabhakaran et al. (2022). The variability of the droplet growth conditions in the Pi Chamber and in the idealized models considered here are attributed to different sources, operating on different spatial scales. In the Pi Chamber [see e.g., Chang et al. (2016)], the variability of the droplet growth conditions are caused by fixed scalar boundary conditions (for temperature and vapor on the chamber walls) that sustain supersaturation fluctuations against isobaric mixing due to Rayleigh-Bénard turbulence. Also, the domain of the Pi Chamber is of relatively small vertical extent compared with typical grid boxes in LES. This rules out any significant variability in the adiabatic cooling rates among droplets (ascending with different turbulent vertical velocities), which is the main source of variability in the droplet growth conditions postulated by the models discussed in this work. Finally, we note that the turbulent condensation models discussed here assume the cloudy volume is effectively unbounded (although the DSD sampling volume is finite) and neglect droplet transport by sedimentation. In the Pi Chamber (which may be regarded as a homogeneous but bounded system) large droplets are removed by sedimentation from the sampling volume. This truncates the right tail of the sampled DSD, despite supersaturation fluctuations being continuously maintained by the boundary conditions.

*Acknowledgments.* I am grateful to Christoph Siewert for his stimulating criticism of the eddy hopping model that motivated this paper. This manuscript benefited from discussions with Prasanth Prabhakaran and Raymond Shaw and was initially drafted during my visit to the Kavli Institute for Theoretical Physics (KITP) at the University of California Santa Barbara, that is sponsored by the National Science Foundation under Grant No. NSF PHY-1748958. I thank Wojciech Grabowski for discussions and for his comments on an earlier version of this paper. I am indebted to Marta Waclawczyk who drew my attention to the simplified Langevin model discussed in Sec. 7. We thank two anonymous reviewers for their comments on the manuscript. This work was partly supported by the Polish National Science Centre (NCN) under Grant No. 2017/25/B/ST10/02383.

*Data availability statement.* The data that support the findings of this study are available from the author upon reasonable request.

## APPENDIX A

### Modified periodic boundary conditions

We sketch here a simple procedure to apply the modified PBC shown schematically in Fig. 4.b. The scheme resembles the so-called Lees-Edwards boundary conditions (Lees and Edwards 1972) used in particle-based molecular dynamics simulations of fluids under shear flow.

Knowing the droplet vertical position  $z(t)$  and its squared radius  $a(t)$  at time  $t$ , first obtain the provisional values  $z_*$  and  $a_*$  at time  $t + \delta t$  by numerical integration of (14) and (7) over the model time step  $\delta t$ . Then correct (if necessary) the provisional values for periodicity to obtain  $z(t + \delta t)$  and  $a(t + \delta t)$  as follows,

$$z(t + \delta t) = z_* + \epsilon \Delta, \quad (\text{A1})$$

and

$$a(t + \delta t) = a_* + \epsilon \gamma_a \Delta, \quad (\text{A2})$$

where

$$\epsilon = \begin{cases} +1, & \text{if } z_* < \langle z \rangle - \Delta/2, \\ -1, & \text{if } z_* > \langle z \rangle + \Delta/2, \\ 0, & \text{otherwise.} \end{cases} \quad (\text{A3})$$

is the periodicity correction index,  $\langle z \rangle$  is the mean vertical position of the droplets of the ensemble, and  $\bar{\gamma}_a$  is the mean vertical gradient of the squared radius  $a$ .

For the eddy hopping model operating in adiabatic parcels we may assume that the vertical structure of  $a$  follows the quasi-steady profile [Eq. (16)] over the length scale  $\Delta$  of the sampling volume and approximate

$$\bar{\gamma}_a \approx 2DA_1\tau_s, \quad (\text{A4})$$

where the phase relaxation time  $\tau_{\text{ph}}$  in  $\tau_s$  is approximated as

$$\tau_{\text{ph}} \approx 1/[A_2\langle\mu_1\rangle_\Delta]. \quad (\text{A5})$$

For DNS-like models of type A, instead of using (A4) and (A5),  $\bar{\gamma}_a$  may be estimated from a least square fit to a linear profile of the droplet squared radius.

## APPENDIX B

### Phase modification and supersaturation spectrum

The Fourier-Laplace transforms  $S(\omega)$  and  $w(\omega)$  of  $S(t)$  and  $w(t)$  are linearly related through the transfer function  $\varphi(\omega) = \varphi'(\omega) + i\varphi''(\omega)$  [Eq. (25)]. It is of interest to write  $\varphi'(\omega)$  and  $\varphi''(\omega)$  in terms of reduced functions of the dimensionless frequency  $\hat{\omega} = \omega\tau_s$ ,

$$R(\hat{\omega}) \equiv \frac{\varphi'(\hat{\omega})}{\varphi'(0)} = \frac{1}{1 + \hat{\omega}^2}, \quad I(\hat{\omega}) \equiv \frac{\varphi''(\hat{\omega})}{\varphi''(0)} = \frac{\hat{\omega}}{1 + \hat{\omega}^2}.$$

The reduced functions are plotted in Fig. B1. The real part  $R(\hat{\omega})$ , which is in phase with the “forcing”  $w(t)$ , dominates the “response”  $S(t)$  in the lower frequency range ( $\hat{\omega} = \omega\tau_s \lesssim 1$ ), but vanishes in the high-frequency regime ( $\hat{\omega} \gtrsim 10$ ). The phase modification due to  $I(\hat{\omega})$  takes place on a range of frequencies around  $1/\tau_s$  (that is,  $\hat{\omega} = 1$ ).

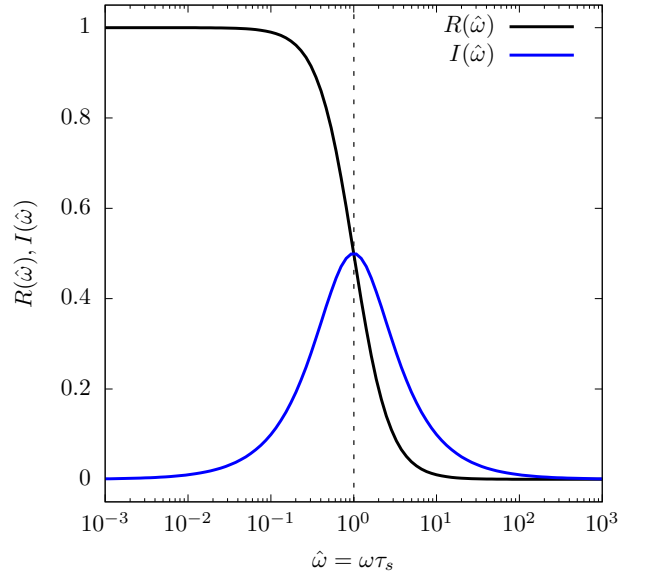


Fig. B1. Reduced functions  $R(\hat{\omega})$  and  $I(\hat{\omega})$  as a function of the dimensionless frequency  $\hat{\omega} = \omega\tau_s$ .

Now let us consider the power spectrum  $E_S(\omega)$  of supersaturation fluctuations  $S(t)$  driven by vertical velocity fluctuations  $w(t)$ . It can be shown that  $E_S(\omega)$  is related to the power spectrum  $E_w(\omega)$  of  $w(t)$  through the transfer function  $\varphi(\omega)$  defined in (25),

$$E_S(\omega) = |\varphi(\omega)|^2 E_w(\omega). \quad (\text{B1})$$

The statistically stationary process  $w(t)$  is described by Eq. (13) and has autocorrelation function

$$R_w(t) = \langle w'(t_0)w'(t_0+t) \rangle = \sigma_w^2 e^{-|t|/\tau_w},$$

with integral time scale  $\tau_w$ . The spectrum  $E_w(\omega)$  is twice the Fourier transform of  $R_w(t)$  and equals [see e.g., Pope (2000)]

$$E_w(\omega) = \frac{1}{\pi} \int_{-\infty}^{\infty} R_w(t) e^{-i\omega t} dt = \frac{2}{\pi} \frac{\sigma_w^2 \tau_w}{1 + \omega^2 \tau_w^2}. \quad (\text{B2})$$

Accordingly,  $E_s(\omega)$  is twice the Fourier transform of  $R_s(t) = \langle S'(t_0)S'(t_0+t) \rangle$  with integral time scale  $\tau_s$ . Then it follows from (B1), (25), and (B2) that

$$E_s(\omega) = \frac{2}{\pi} \frac{A_1^2 \tau_s^2}{1 + \omega^2 \tau_s^2} \frac{\sigma_w^2 \tau_w}{1 + \omega^2 \tau_w^2}.$$

The dimensionless spectrum  $\hat{E}_s(\hat{\omega})$ , scaled by  $(2/\pi)A_1^2\tau_s^2\sigma_w^2\tau_w$ , in terms of the dimensionless frequency  $\hat{\omega} = \omega\tau_s$ , is,

$$\hat{E}_s(\hat{\omega}) = \frac{1}{1 + \hat{\omega}^2} \frac{1}{1 + (\hat{\omega}/\alpha)^2}, \quad (\text{B3})$$

where  $\alpha = \tau_s/\tau_w$  is the ratio of the integral time scales of  $S(t)$  and  $w(t)$ .

## APPENDIX C

### Equations for DNS-like models

In general, DNS studies of turbulent condensation solve the Navier-Stokes (NS) equations<sup>7</sup> for the velocity field  $\mathbf{u}$ ,

$$\partial_t \mathbf{u} = \dots + \mathbf{f}, \quad \nabla \cdot \mathbf{u} = 0, \quad (\text{C1})$$

where on the right-hand side (RHS) we omit the convective acceleration and the well-known NS terms, making explicit only the external statistically homogeneous and isotropic momentum forcing  $\mathbf{f}$ . It is applied on the larger scales  $\sim \Delta$  of the computational box to maintain a turbulent stationary flow. This momentum forcing mimics turbulence production by scales larger than  $\Delta$  and is a common feature of all DNS studies.

The treatment of thermodynamics and moisture, however, differ among various DNS studies. Some models resolve both the temperature  $T$  and the vapor mixing ratio  $q$  as the thermodynamic prognostic variables. The local changes of  $q$  and  $T$  are described by equations of the form,

$$\partial_t q = f_q + \dots, \quad (\text{C2})$$

and

$$\partial_t T = -\Gamma w + f_T + \dots, \quad (\text{C3})$$

where  $\Gamma = g/c_p$  is the lapse rate accounting for the adiabatic cooling effect,  $w = \mathbf{u} \cdot \hat{\mathbf{e}}_z$  is the local vertical velocity,  $f_q$  and  $f_T$  are large-scale stochastic forcing of the vapor and temperature fields. The dots on the RHS of (C2) and (C3) represent other contributions, such as advection by the resolved turbulent field  $\mathbf{u}$ , molecular diffusion and condensation (accompanied by latent heat exchanges). The local supersaturation  $S$  specifying the ambient conditions for droplet growth is diagnosed from  $T$  and  $q$ .

Other DNS studies do not resolve  $T$  or  $q$ , but directly compute the supersaturation  $S$  driving droplet growth by condensation. In this  $S$ -formulation for the thermodynamic scalars, the supersaturation obeys an equation of the form

$$\partial_t S = A_1 w + f_S + \dots, \quad (\text{C4})$$

where  $f_S$  stands for the large-scale supersaturation forcing and  $A_1$  is the coefficient [same as in Eq. (4)] accounting for the adiabatic cooling effect. Again, the dots on the RHS of (C4) represent turbulent advection by  $\mathbf{u}$ , molecular diffusion and condensation. The RHS of the equations above for  $T$ ,  $q$ , and  $S$  makes explicit only the ‘‘external’’ stochastic sources producing fluctuations in the thermodynamics scalars (other than small-scale fluctuations due to the nonlinear cascade) that lead to variability in droplets growth conditions.

DNS studies of type B neglect the adiabatic cooling effect by assuming  $\Gamma = 0$  (or  $A_1 = 0$  in the  $S$ -formulation), and simulate supersaturation fluctuations solely produced by the scalar forcing at large scales  $\sim \Delta$ ; hence they assume  $f_T \neq 0$  and  $f_q \neq 0$  in (C3) and (C2) [or  $f_S \neq 0$  in the  $S$ -formulation (C4)].

DNS studies of type A do not apply any large-scale scalar forcing. Hence they assume  $f_T = f_q = 0$  in (C3) and (C2) [or  $f_S = 0$  in (C4)] and rely on the local adiabatic cooling effect driven by vertical velocity fluctuations ( $\Gamma \neq 0$  or  $A_1 \neq 0$ ) as the only source of supersaturation variability.

## References

- Abade, G. C., and D. G. Albuquerque, 2024: Persistent mixed-phase states in adiabatic cloud parcels under idealised conditions. *Quarterly Journal of the Royal Meteorological Society*, **150** (763), 3450–3474.
- Abade, G. C., W. W. Grabowski, and H. Pawlowska, 2018: Broadening of cloud droplet spectra through eddy hopping: turbulent entrainment parcel simulations. *J. Atmos. Sci.*
- Arabas, S., A. Jaruga, H. Pawlowska, and W. W. Grabowski, 2015: libcloudph++ 1.0: a single-moment bulk, double-moment bulk, and particle-based warm-rain microphysics library in C++. *Geosci. Model Dev.*, **8** (6), 1677–1707, <https://doi.org/10.5194/gmd-8-1677-2015>.

- Bartlett, J. T., and P. R. Jonas, 1972: On the dispersion of the sizes of droplets growing by condensation in turbulent clouds. *Quarterly Journal of the Royal Meteorological Society*, **98** (415), 150–164.

<sup>7</sup>Some studies [e.g., Paoli and Shariff (2009)] solve the equations for compressible fluid motion. However, this feature is not relevant for the present discussion.

- Celani, A., G. Falkowich, A. Mazzino, and A. Seminara, 2005: Droplet condensation in turbulent flows. *70* (6), 775–781.
- Celani, A., A. Mazzino, and M. Tizzi, 2008: The equivalent size of cloud condensation nuclei. *New J. Phys.*, **10** (7), 075 021.
- Celani, A., A. Mazzino, and M. Tizzi, 2009: Droplet feedback on vapor in a warm cloud. *Int. J. Mod. Phys. B*, **23** (28 & 29), 5434–5443.
- Chandrakar, K. K., W. Cantrel, K. C. Chang, D. Ciochetto, D. Niedermeier, M. Ovchinnikov, R. A. Shaw, and F. Yang, 2016: Aerosol indirect effect from turbulence-induced broadening of cloud-droplet size distributions. *Proc. Natl. Acad. Sci. (USA)*, **113** (50), 14 243–14 248.
- Chandrakar, K. K., W. W. Grabowski, H. Morrison, and G. H. Bryan, 2021: Impact of entrainment mixing and turbulent fluctuations on droplet size distributions in a cumulus cloud: An investigation using lagrangian microphysics with a subgrid-scale model. *Journal of the Atmospheric Sciences*, **78** (9), 2983 – 3005.
- Chandrakar, K. K., H. Morrison, and R. A. Shaw, 2023: Lagrangian and eulerian supersaturation statistics in turbulent cloudy rayleigh–bénard convection: Applications for les subgrid modeling. *Journal of the Atmospheric Sciences*, **80** (9), 2261 – 2285.
- Chang, K., and Coauthors, 2016: A laboratory facility to study gas–aerosol–cloud interactions in a turbulent environment: The  $\pi$  chamber. *Bulletin of the American Meteorological Society*, **97** (12), 2343 – 2358.
- Clark, T. L., and W. D. Hall, 1979: A numerical experiment on stochastic condensation theory. *Journal of Atmospheric Sciences*, **36** (3), 470 – 483.
- Cooper, W. A., 1989: Effects of variable droplet growth histories on droplet size distributions. Part I: Theory. *J. Atmos. Sci.*, **46** (10), 1301–1311.
- Dziekan, P., and H. Pawlowska, 2017: Stochastic coalescence in lagrangian cloud microphysics. *Atmospheric Chemistry and Physics*, **17** (22), 13 509–13 520.
- Dziekan, P., M. Waruszewski, and H. Pawlowska, 2019: University of warsaw lagrangian cloud model (uwlcmm) 1.0: a modern large-eddy simulation tool for warm cloud modeling with lagrangian microphysics. *Geoscientific Model Development*, **12** (6), 2587–2606, <https://doi.org/10.5194/gmd-12-2587-2019>.
- Germano, M., 1992: Turbulence: the filtering approach. *Journal of Fluid Mechanics*, **238**, 325–336.
- Gillespie, D. T., 1972: The stochastic coalescence model for cloud droplet growth. *Journal of Atmospheric Sciences*, **29** (8), 1496 – 1510.
- Grabowski, W. W., and G. C. Abade, 2017: Broadening of cloud droplet spectra through eddy hopping: Turbulent adiabatic parcel simulations. *J. Atmos. Sci.*, **74**, 1485–1493.
- Grabowski, W. W., and L. Thomas, 2021: Cloud droplet diffusional growth in homogeneous isotropic turbulence: bin microphysics versus lagrangian super-droplet simulations. *Atmospheric Chemistry and Physics*, **21** (5), 4059–4077.
- Grabowski, W. W., L. Thomas, and B. Kumar, 2022a: Impact of cloud-base turbulence on ccn activation: Ccn distribution. *Journal of the Atmospheric Sciences*, **79** (11), 2965 – 2981.
- Grabowski, W. W., L. Thomas, and B. Kumar, 2022b: Impact of cloud-base turbulence on CCN activation: Single-size CCN. *J. Atmos. Sci.*, **79** (2), 551 – 566.
- Hoffmann, F., and G. Feingold, 2019: Entrainment and mixing in stratocumulus: Effects of a new explicit subgrid-scale scheme for large-eddy simulations with particle-based microphysics. *J. Atmos. Sci.*, **76** (7), 1955–1973.
- Hoffmann, F., T. Yamaguchi, and G. Feingold, 2019: Inhomogeneous mixing in lagrangian cloud models: Effects on the production of precipitation embryos. *J. Atmos. Sci.*, **76** (1), 113–133.
- Kabanov, A. S., I. P. Mazin, and V. I. Smirnov, 1971: Comment on “the theory of growth of cloud drops by condensation”. *Journal of Atmospheric Sciences*, **28** (1), 129 – 130.
- Kerstein, A. R., 1988: A linear-eddy model of turbulent scalar transport and mixing. *Combustion Science and Technology*, **60** (4-6), 391–421.
- Khvorostyanov, V. I., and J. Curry, 1999: Toward the theory of stochastic condensation in clouds. Part I: A general kinetic equation. *J. Atmos. Sci.*, **56**, 3985–3996.
- Krueger, S. K., C.-W. Su, and P. A. McMurty, 1997: Modeling entrainment and finescale mixing in cumulus clouds. *J. Atmos. Sci.*, **54** (23), 2697–2712.
- Lanotte, A. S., A. Seminara, and F. Toschi, 2009: Cloud droplet growth by condensation in homogeneous isotropic turbulence. *J. Atmos. Sci.*, **66** (6), 1685–1697, <https://doi.org/10.1175/2008JAS2864.1>.
- Lees, A. W., and S. F. Edwards, 1972: The computer study of transport processes under extreme conditions. *Journal of Physics C: Solid State Physics*, **5** (15), 1921.
- Lemons, D. S., 2002: *An introduction to stochastic processes in physics*. Johns Hopkins University Press.
- MacInnes, J. M., and F. V. Bracco, 1992: Stochastic particle dispersion modeling and the tracer-particle limit. *Physics of Fluids A: Fluid Dynamics*, **4** (12), 2809–2824.
- Manton, M. J., 1979: On the broadening of a droplet distribution by turbulence near cloud base. *Quarterly Journal of the Royal Meteorological Society*, **105** (446), 899–914.
- Paoli, R., and K. Shariff, 2009: Turbulent condensation of droplets: direct simulation and a stochastic model. *J. Atmos. Sci.*, **66**, 723.
- Pope, S. B., 1994: Lagrangian pdf methods for turbulent flows. *Annual Review of Fluid Mechanics*, **26** (Volume 26, 1994), 23–63.
- Pope, S. B., 2000: *Turbulent flows*. Cambridge University Press.
- Pope, S. B., 2011: Simple models of turbulent flows. *Physics of Fluids*, **23** (1), 011 301.
- Prabhakaran, P., S. Thomas, W. Cantrell, R. A. Shaw, and F. Yang, 2022: Sources of stochasticity in the growth of cloud droplets: Supersaturation fluctuations versus turbulent transport. *Journal of the Atmospheric Sciences*, **79** (12), 3145 – 3162.
- Résibois, P., and M. De Leener, 1977: *Classical Kinetic Theory of Fluids*. John Wiley & Sons.
- Rodean, H. C., 1996: *Stochastic Lagrangian models of turbulent diffusion*. American Meteorological Society.

- Saito, I., and T. Gotoh, 2018: Turbulence and cloud droplets in cumulus clouds. *New Journal of Physics*, **20** (2), 023 001.
- Saito, I., T. Gotoh, and T. Watanabe, 2019: Broadening of cloud droplet size distributions by condensation in turbulence. *J. Meteor. Soc. Japan*, **97** (4), 867–891.
- Saito, I., T. Watanabe, and T. Gotoh, 2021: Statistical properties of a stochastic model of eddy hopping. *Atmospheric Chemistry and Physics*, **21** (17), 13 119–13 130.
- Sardina, G., F. Picano, B. L., and R. Caballero, 2015: Continuous growth of droplet size variance due to condensation in turbulent clouds. *Phys. Rev. Lett.*, **115**, 184 501.
- Sardina, G., S. Poulain, B. L., and R. Caballero, 2018: Broadening of cloud droplet size spectra by stochastic condensation: effects of mean updraft velocity and CCN activation. *J. Atmos. Sci.*, **75**, 451–467.
- Shaw, R. A., 2003: Particle-turbulence interactions in atmospheric clouds. *Annual Review of Fluid Mechanics*, **35** (1), 183–227.
- Shima, S., K. Kusano, A. Kawano, T. Sugiyama, and S. Kawahara, 2009: The super-droplet method for the numerical simulation of clouds and precipitation: A particle-based and probabilistic microphysics model coupled with a non-hydrostatic model. *Q. J. R. Meteorol. Soc.*, **135**, 1307–1320.
- Siewert, C., J. Bec, and G. Krstulovic, 2017: Statistical steady state in turbulent droplet condensation. *J. Fluid Mech.*, **810**, 254–280, <https://doi.org/10.1017/jfm.2016.712>.
- Thomas, L., W. W. Grabowski, and B. Kumar, 2020: Diffusional growth of cloud droplets in homogeneous isotropic turbulence: DNS, scaled-up DNS, and stochastic model. *Atmos. Chem. Phys.*, **2020**, 1–21.
- Vaillancourt, P. A., M. K. Yau, P. Bartello, and W. W. Grabowski, 2002: Microscopic approach to cloud droplet growth by condensation. Part II: Turbulence, clustering, and condensational growth. *J. Atmos. Sci.*, **59** (24), 3421–3435, [https://doi.org/10.1175/1520-0469\(2002\)059<3421:MATCDG>2.0.CO;2](https://doi.org/10.1175/1520-0469(2002)059<3421:MATCDG>2.0.CO;2).
- Weil, J. C., P. P. Sullivan, and C.-H. Moeng, 2004: The use of large-eddy simulations in lagrangian particle dispersion models. *Journal of the Atmospheric Sciences*, **61** (23), 2877 – 2887.